AD NUMBER: AD0337904
CLASSIFICATION CHANGES
TO: Unclassified
FROM: Confidential
LIMITATION CHANGES
TO: Approved for public release; distribution is unlimited.
FROM: Distribution authorized to U.S. Government Agencies and their Contractors; Administrative/Operational Use; 6 Dec 1957. Other requests shall be referred to Defense Nuclea Agency, Washington, DC 20301.
AUTHORITY
U per DNA ltr dtd 28 Feb 1980; ST-A per DODD 5200.2 dtd 11 Dec 1997

~~CONFIDENTIAL~~

PRELIMINARY REPORT

ITR-1409

This document consists of 50 pages.

No. 155 of 215 copies, Series A

OPERATION

PLUMB BOB

NEVADA TEST SITE

MAY-OCTOBER 1957

Project 1.8c

AIR-BLAST PHENOMENA AS AFFECTED BY TERRAIN

HEADQUARTERS FIELD COMMAND,
ARMED FORCES SPECIAL WEAPONS PROJECT
SANDIA BASE, ALBUQUERQUE, NEW MEXICO

FORMERLY RESTRICTED DATA

Handle as Restricted Data in foreign dissemination. Section 144b, Atomic Energy Act of 1954.

This material contains information affecting the national defense of the United States within the meaning of the espionage laws Title 18, U. S. C., Secs. 793 and 794, the transmission or revelation of which in any manner to an unauthorized person is prohibited by law.

This is a preliminary report based on all data available at the close of this project's participation in Operation PLUMBBOB. The contents of this report are subject to change upon completion of evaluation for the final report. This preliminary report will be superseded by the publication of the final (WT) report. Conclusions and recommendations drawn herein, if any, are therefore tentative. The work is reported at this early time to provide early test results to those concerned with the effects of nuclear weapons and to provide for an interchange of information between projects for the preparation of final reports.

When no longer required, this document may be destroyed in accordance with applicable security regulations. When destroyed, notification should be made to

AEC Technical Information Service Extension
P. O. Box 401
Oak Ridge, Tenn.

DO NOT RETURN THIS DOCUMENT

AEC Technical Information Service Extension
Oak Ridge, Tennessee

(4) NA (5) 829800 7NA 8-1760 cy1

REG. NO. 18986 CONFIDENTIAL (8) U

LOG. NO. 22132

WDSOT

ITR-1409

OPERATION PLUMBBOB—PROJECT 1.8c

(6)

AIR-BLAST PHENOMENA AS AFFECTED BY TERRAIN, [U]

(10) by L. M. Swift and
D. C. Sachs,

Stanford Research Institute
Menlo Park, California

(11)

Issuance Date: December 6, 1957

(12) 50 p.
(13) NA
(14 & 15) NA
(16) Pegs. 1.8c
4-15-58
107-(1) mnl
202-1-17 (17) NA
(18) AEC
(19) ITR-1409
(20) C
(21) Report on Operation Plumbbob [U]

FORMERLY RESTRICTED DATA

Handle as Restricted Data in foreign dissemination. Section 144b, Atomic Energy Act of 1954.

This material contains information affecting the national defense of the United States within the meaning of the espionage laws, Title 18, U.S.C., Secs. 793 and 794, the transmission or revelation of which in any manner to an unauthorized person is prohibited by law.

John W. Kodis
J. W. Kodis, Lt Col, USAF
Director, Program 1

K. D. Coleman
K. D. Coleman, Col, USAF
Test Group Director, Programs 1–9

Fdc CONFIDENTIAL

ABSTRACT

The objective of Project 1.8c was to obtain data on the effects of gross variations of terrain upon a blast wave produced by a nuclear explosion, particularly at ground ranges of importance to moderately hard targets. On Shot Smoky (48 kt, 700-foot height of burst), total-head pressure, pitot-tube dynamic pressure, and overpressure were measured (1) on both sides of a ridge that rose 280 feet to a crest about 2,600 feet from ground zero and (2) at several equivalent ground ranges along relatively smooth terrain. ~~(for comparison with Item 1).~~

~~Results indicate that~~ a precursor formed over both the flat and ridge blast lines. The wave forms are not pure types and do not lend themselves to definite classification. Surface-level wave-front-propagation velocities indicate enhanced thermal effects on the front slope of the ridge and a strong diffraction effect as the wave passed over the top of the ridge.

~~Although there is evidence that surface level overpressure near the top of the ridge was depressed significantly,~~ generally, the ridge appeared to provide no real protection from overpressure, with increased overpressures noted on the front face and near the bottom of the back slope. However, the ridge appeared to offer considerable protection to drag-sensitive targets along the back slope and at the foot of the back slope.

No significant pressure spikes were observed on the ridge line; the precursor-type blast wave probably prohibited this effect. (C)

FOREWORD

This report presents the preliminary results of one of the 43 projects comprising the Military Effects Program of Operation Plumbbob, which included 28 test detonations at the Nevada Test Site in 1957.

For overall Plumbbob military-effects information, the reader is referred to the "Summary Report of the Director, DOD Test Group (Programs 1–9)," ITR–1445, which includes: (1) a description of each detonation, including yield, zero-point location and environment, type of device, ambient atmospheric conditions, etc.; (2) a discussion of project results; (3) a summary of the objectives and results of each project; and (4) a listing of project reports for the Military Effects Program.

PREFACE

The planning and execution of Project 1.8 c were under the direction of L. M. Swift, with L. H. Inmann serving as field party chief and W. M. Wells as assistant to the project leader. Other members of the field party included H. Wuner, C. M. Westbrook, R. V. Ohler, V. E. Krakow, and R. E. Aumiller. Miss Phyllis Flanders and Miss Diane Smithem assisted in report preparation.

The cooperation and aid of Major H. T. Bingham, USAF, and Lt. Col. J. R. Kodis, USAF, are gratefully acknowledged.

CONTENTS

ABSTRACT ---- 5

FOREWORD ---- 6

PREFACE ---- 6

CHAPTER 1 INTRODUCTION ---- 9

1.1 Objectives ---- 9
1.2 Background ---- 9
1.3 Theory ---- 10

CHAPTER 2 EXPERIMENT PLAN AND PREDICTIONS ---- 13

2.1 Gage Layout ---- 13
2.2 Predictions ---- 13
2.2.1 Flat-Line Predictions ---- 15
2.2.2 Ridge-Line Predictions ---- 17

CHAPTER 3 INSTRUMENTATION ---- 20

3.1 Shot Participation ---- 20
3.2 Central Station ---- 20
3.3 Transducers ---- 21
3.3.1 Blast Gages ---- 21
3.3.2 Subsonic Pitot-Tube Gages ---- 21
3.3.3 Supersonic Total-Head Gage ---- 22
3.3.4 Gage Towers ---- 22
3.4 Gage Coding ---- 23
3.5 Instrument Response ---- 23
3.6 Calibration ---- 25

CHAPTER 4 OPERATIONS ---- 26

CHAPTER 5 RESULTS ---- 27

5.1 Instrument Performance ---- 27
5.2 Data Reduction ---- 27
5.3 Gage Records ---- 27

CHAPTER 6 DISCUSSION ---- 35

6.1 Wave-Form Classification ---- 35
6.2 Overpressure ---- 35
6.3 Dynamic Pressure ---- 37
6.4 Arrival Time and Propagation Velocity ---- 38
6.5 Flat-Line Comparisons ---- 39
6.6 Indications of Asymmetry ---- 43

CHAPTER 7 CONCLUSIONS ---- 45

APPENDIX OVERPRESSURE WAVE-FORM CLASSIFICATION ---- 46

REFERENCES ---- 48

FIGURES

1.1 Peak pressure ratio versus slope angle for rising slopes ---- 11
1.2 Pressure ratios for 20-degree slopes ---- 11
2.1 Layout of gage stations ---- 14
2.2 Profile of gage lines ---- 16
2.3 Met and Priscilla results, scaled to Smoky ---- 18
2.4 Smoky predictions ---- 18
3.1 Modified head for Sandia-Wiancko pitot-tube gage ---- 21
3.2 SRI supersonic total-head gage ---- 22
3.3 Typical gage installation, front slope ---- 23
3.4 Typical gage installation, top of ridge ---- 24
3.5 Typical gage installation, back slope ---- 24
5.1 Surface-level overpressure, Line 1 ---- 28
5.2 Surface-level overpressure, Line 3 ---- 29
5.3 Overpressures at surface, 3-foot, and 10-foot levels, Line 3 ---- 30
5.4 Total-head pressure and pitot-tube dynamic pressure, Line 1 ---- 32
5.5 Total-head pressure and pitot-tube dynamic pressure, Line 3 ---- 33
6.1 Height of burst for surface-level-overpressure wave forms ---- 36
6.2 Peak overpressure versus ground range ---- 40
6.3 Peak dynamic pressure versus ground range ---- 41
6.4 Arrival time versus ground range ---- 42
6.5 Propagation velocity versus ground range ---- 42
6.6 Measured peak overpressure compared with TM 23-200 ---- 43
6.7 Measured peak dynamic pressure compared with Priscilla and Met data ---- 44

TABLES

2.1 Gage Layout ---- 15
2.2 Comparison of Shot Data ---- 17
5.1 Overpressure ---- 34
5.2 Dynamic Pressure ---- 34
6.1 Wave Front Velocity, Smoky ---- 39

Chapter 1

INTRODUCTION

1.1 OBJECTIVES

The objective of Project 1.8c was to obtain data on the effects of gross variation of terrain upon a blast wave produced by a nuclear explosion, particularly at ground ranges of importance to moderately hard targets. Specifically, this project measured air-blast phenomena from Shot Smoky (originally planned as 45 kt, 700-foot height of burst) on both sides of a ridge that rose 280 feet to a crest about 2,600 feet from ground zero and at several ground ranges along relatively smooth terrain. These data were to be interpreted and correlated with similar measurements made by Project 1.8a and with data from other nuclear tests.

1.2 BACKGROUND

It is obvious that gross variations of terrain will modify appreciably the characteristics of blast waves passing over these obstructions. Experience with high-explosives qualitatively confirms this observation, and revetments, etc., have long been used for protection against explosive devices. Revetments of normal sizes are not found as useful against nuclear blasts as they are for chemical explosives, because of the larger relative dimensions of the nuclear blast wave. Observations of the damage at Nagasaki, however, show evidence of change of blast effects by natural terrain.

Full-scale observations of these effects have heretofore been limited to very low-pressure regions by the fact that normal operations of nuclear tests in Nevada have placed shot points at considerable distances from the surrounding mountains. During Operation Tumbler–Snapper, Project 19.18 (Reference 1) instrumented a ridge approximately 17,000 feet from Shot 5; during Operation Upshot–Knothole, Project 1.1c (Reference 2) instrumented the same region for Shot 7, at the same shot point in Area 1. On both of these projects the peak (undisturbed) pressure level was less than 3 psi, and measurements were made only of overpressure at the earth's surface.

The data obtained from these projects show that a low-pressure shock wave is indeed modified markedly by changes in slope of the terrain. The wave form is markedly changed, initial spikes being formed on the up-hill side and in the region where the down-hill side flattens out, with rounded wave forms on the initial down-hill side. Peak pressures are markedly increased on the up-hill side and depressed on the down-hill side.

Data taken by Project 3.6 of Operation Teapot (Reference 3) may be considered an idealized model of this problem, although the dimensions of the structure studied were relatively small. The shape consisted of an earth fill of trapezoidal cross section approximately 15 feet high and 100 feet long with front and back slopes of about 0.5 (θ = 26 degrees). It was located 1,500 feet from the ground zero of Shot Met (22 kt), in a region of strong precursor effects. The project objective was to determine structural response of the earth-

covered structure; pressure-time measurements were taken to describe the loading.

The few records of surface overpressure obtained show that the front-slope surface pressures, as measured, were intermediate between the free-field overpressure (p) and the free-field dynamic pressure (q) but resembled neither in wave form. As a rough average over the first 200 msec, a value of $p + 0.25q$ was ascribed to these results. These Teapot measurements were necessarily taken very near the beginning of the slope, however, compared with the problem at hand—i.e., where the change in slope was quite abrupt. It is possible that the flow patterns were markedly different from those to be expected on a larger slope.

Pressures on the rear slope of the Teapot 3.6 structure were reported as trivial, being much lower than free-field overpressure.

The WADC Technical Report 56-284 (Reference 4) gives most of the available analytical background for preduction of the effects of slopes on air blasts. However, it considers shock waves exclusively and deals only with surface overpressure. No background analytical or experimental data appears to exist on the effects of slope in the precursor or with regard to dynamic pressure, except the previously mentioned meager information obtained by Teapot Project 3.6.

1.3 THEORY

When an explosive charge is fired at a height above a flat surface, a Mach stem is formed as the angle of incidence passes a certain critical angle, roughly 40 degrees from the vertical. Beyond the point of formation of the Mach stem, the blast wave near the surface propagates as a cylindrical wave, with the shock front normal to the surface. With minor exceptions, the conditions in the blast wave at moderate pressure levels are then no longer a function of the burst height. If this vertical Mach stem reaches a point where the surface changes to a rising slope, a new Mach stem is formed perpendicular to the new slope, with an accompanying increase in peak pressure. The new stem forms a triple point with the old, which rises rapidly from the surface. The ratio of the increased peak overpressure to the original peak overpressure is a function of the slope angle (or more properly the change in slope) and of the original pressure. At angles up to the critical angle, the Mach reflection coefficient is greater for low pressure than for high, in contrast to the inverse condition for greater angles.

If the Mach stem passes over a convex surface to a falling slope, no such new stem is formed; diffraction takes place, and the peak pressures tend to be reduced.

These phenomena are independent of the original burst height if the Mach stem has formed before the change in slope is reached. The shielding effect of terrain is therefore not the simple matter of obstructing the direct line between the burst and the target.

In the case of relatively low nuclear bursts, the formation of the Mach stem is frequently obscured by the formation of a precursor, with slow rise times and disturbed wave forms, which persists out to considerable distances, so that the foregoing remarks are only roughly applicable. However, since the clean classical shock wave is the only one subject to mathematical treatment and to small-scale study, it is profitable to consider further the effects of terrain on clean waves.

Broadview Research and Development (Reference 4), in considering the effects of rising slopes, presents a family of empirical curves of peak pressure ratio versus slope angle for a variety of pressure levels. These curves are partly reproduced in Figure 1.1, where peak-pressure ratio is defined as the ratio of the peak pressure observed on a rising slope preceded by a flat region to that observed at the same ground range on a flat surface. It is obvious from the figure that the pressure ratio (PR) tends to vary inversely

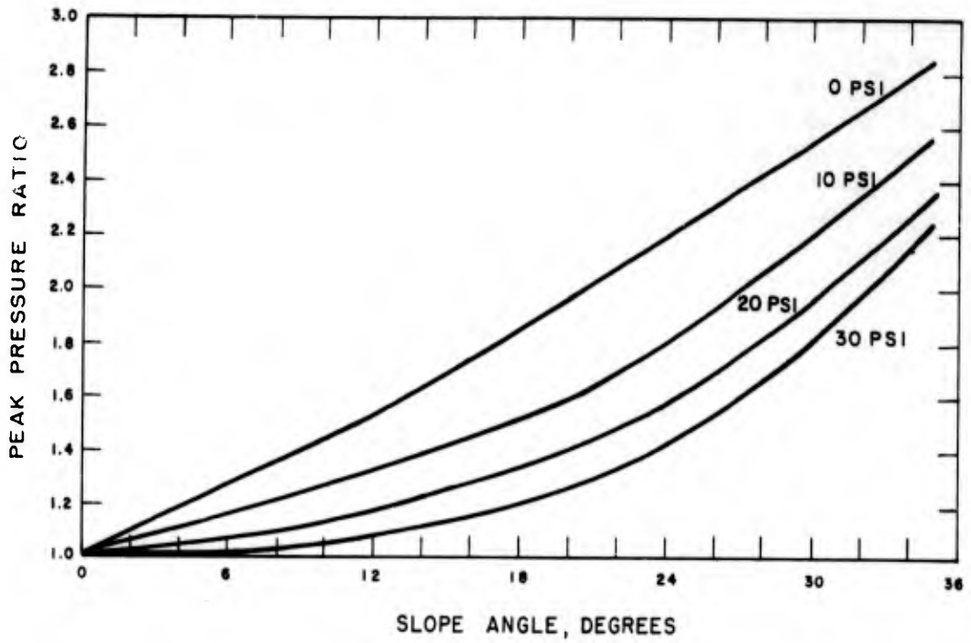

Figure 1.1 Peak pressure ratio versus slope angle for rising slopes.

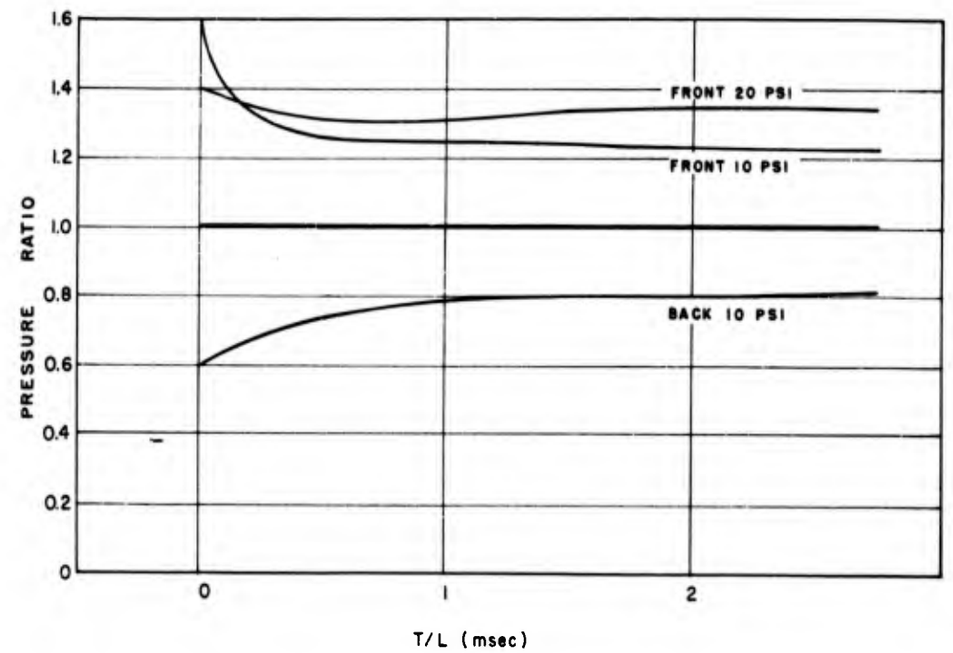

Figure 1.2 Pressure ratios for 20-degree slopes.

with the pressure; in other words, the effect of a rising slope on peak pressure ratio is most pronounced at low pressures.

These curves, however, refer to the peak pressure in a decaying classical shock wave. The effect of the slope in this case is to produce a sharp initial pressure spike of very short duration near the change in slope; this pressure spike increases in duration as the shock traverses up the slope. In terms of pressure versus time, behind the pressure spike there is still a pressure increase over the normal instantaneous overpressure, but the pressure ratio at these times is not as great as the peak-pressure ratio.

Figure 1.2, derived from Reference 4, shows curves of pressure ratio versus normalized time for input pressures of 10 and 20 psi on a 20-degree rising slope. The basis of time normalization is milliseconds of time after shock arrival per foot of distance from the start of the slope to the point of measurement. It is important to note that at 10-psi input pressure the pressure ratio changes much more severely and abruptly with time after shock arrival than does the 20-psi curve. In fact, after t/L exceeds $\frac{1}{8}$, the pressure ratio is higher for the higher pressure.

If the input pressure signal is not a shock wave, but a typical precursor wave form with a slow rise time, it is probable that the spike will not occur. In this case, the average pressure is more important than the peak-pressure ratio derived from Figure 1.1. From Figure 1.2, these average pressure ratios for a 20-degree front slope are about 1.35 for 20 psi and about 1.25 for 10 psi. It seems reasonable to assume that at input levels above 20 psi, the average pressure ratio does not exceed 1.35, since the peak-pressure ratio drops below this figure at about 25 psi. The conclusion reached from these observations is that, for a front slope of about 20 degrees, the peak-pressure ratio to be expected from a precursor-type blast wave will not exceed 1.35, from hydrodynamic effects.

Reference 4 does not present a family of curves similar to those of Figure 1.1 for back slopes. The data, however, from which the lower curve of Figure 1.2 is constructed indicate that the shape of this curve is not extremely dependent on pressure level. Here, again, the average pressure ratio is considered to be important, and an average pressure of 0.75 is considered to be probably applicable to precursor-type waves on a falling slope of 20 degrees.

Chapter 2

EXPERIMENT PLAN AND PREDICTIONS

2.1 GAGE LAYOUT

The gage layout (Figure 2.1 and Table 2.1) for Project 1.8c was designed to cover the regions of interest as thoroughly as possible within the limitations of the total available channels. Line 3 (Stations 31 through 36, inclusive) was chosen to run from ground zero over a ridge approximately 300 feet high and down the back side. The orientation of the line was changed at the top of the ridge to avoid undesirable side slopes. Figure 2.1 indicates that a straight-line continuation would tend to follow along the slope, rather than down hill. A profile of the line is shown in Figure 2.2. Station 34 was selected at the top of the ridge, Stations 33 and 32 at locations near the middle and front edge of the front slope. Station 31 was chosen to be on a relatively uniform slope extending all the way to ground zero. In a similar manner, Stations 35 and 36 were laid out on the back slope of the ridge.

Line 1 (Stations 11 through 15, inclusive) was selected as a reference line to represent as nearly as possible a blast line free from terrain disturbances. Stations were chosen at the same ground ranges as corresponding stations on Line 3 so that direct comparisons could be made. On each of these lines, Project 1.8a installed gages at some similar ground ranges and at more-remote ranges to provide backup and extended data. Project 1.8a also instrumented still other lines, including one over a ridge having a more-extreme slope than that instrumented by Project 1.8c.

A surface-level blast gage (see Section 3.3.1) was installed at each station. At Stations 31, 32 and 33, where very-high dynamic pressures were expected, supersonic total-head gages (see Section 3.3.3), mounted at a height of 3 feet, were used. At Stations 34, 35, and 36, subsonic pitot-tube gages at 3-foot and 10-foot heights were used.

Instrumentation installed on Line 1 omitted the measurement of dynamic pressure at the first station and omitted the station at 2,943 feet, ground range, entirely. On this line, the usual additional channel measuring overpressure at the side ports of the pitot-tube gage was omitted to conserve channels.

For information as to possible instrument damage and for general information on structural response, an accelerometer was mounted inside the recording shelter to measure vertical acceleration. At the frequencies expected, the shelter may be considered to move as a unit, so that one measurement can be used to describe the motion of the shelter as a whole.

2.2 PREDICTIONS

In planning an experiment of this type, it is necessary to predict the magnitudes of the phenomena expected with a reasonable degree of accuracy to set properly gage ranges and attenuators to produce a satisfactory record. In some cases, it is profitable to spend a considerable amount of analytical effort on predictions in an attempt to be as precise as possible, especially when a comparison of results with predictions permits evaluation of an analytical approach based on theory or previous data. In this project, such an approach was considered unprofitable. Neither theory nor experimental data was available for accurate pre-

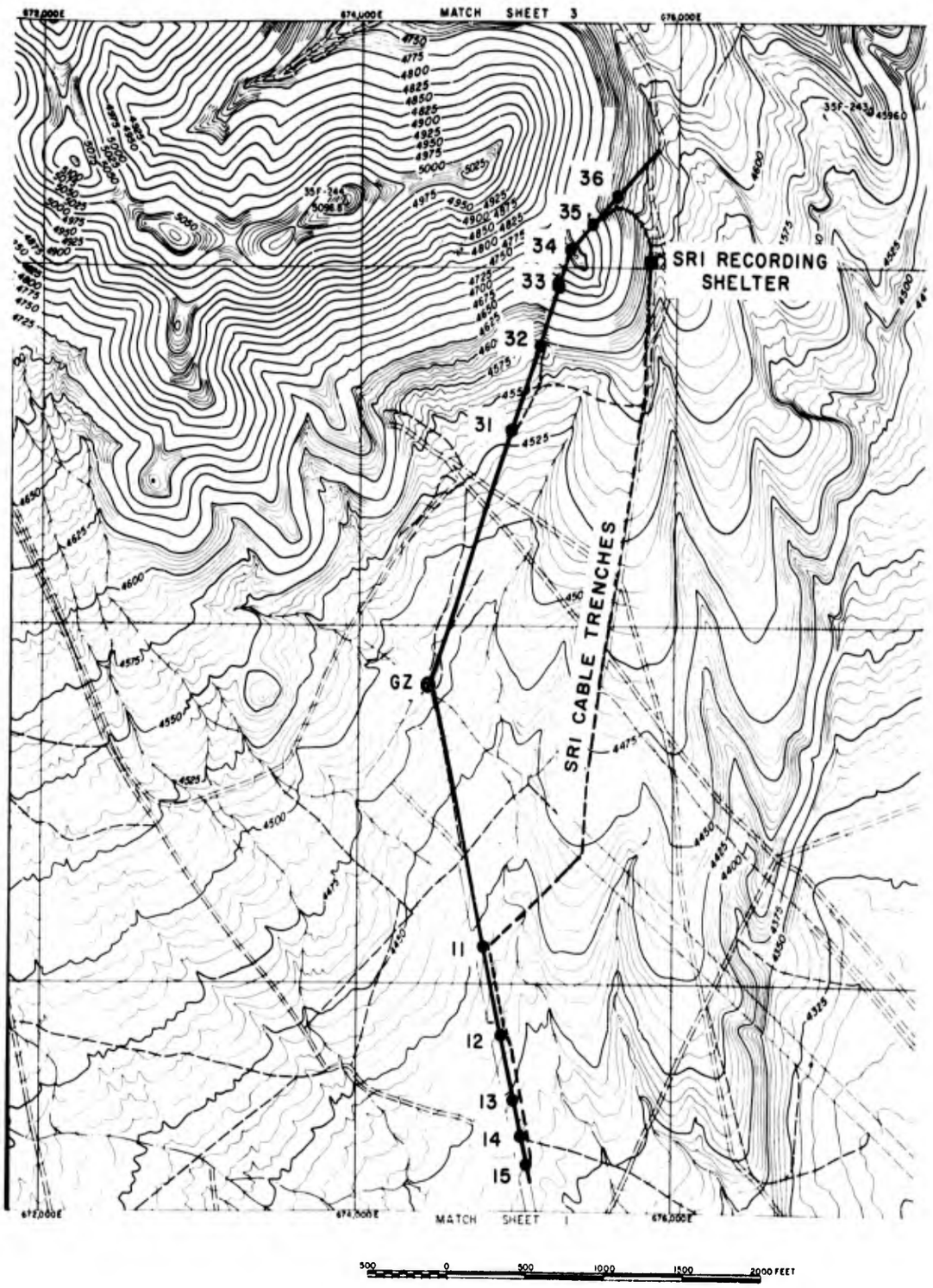

Figure 2.1 Layout of gage stations.

dictions of the terrain effects being studied. Predictions were considered satisfactory if they proved to be within a factor of 2 to 1 of the recorded data.

2.2.1 Flat-Line Predictions. The expected phenomena on Line 1 could be predicted simply with reasonable certainty from the results of Teapot Met (Reference 5) and Plumbbob Priscilla (Reference 6). The comparative data on these shots and Smoky (as originally planned) are shown in Table 2.2.

The close similarity between Shots Priscilla and Smoky is obvious, but the difference

TABLE 2.1 GAGE LAYOUT

Ground Range	Gage Code	Predicted Peak	Gage Rating
feet		psi	
1,501	11B	51	100
2,018	12B	27	100
2,018	12Z3	184	500 *
2,381	13B	18	30
2,381	13Z3	110	200 *
2,589	14B	15	30
2,589	14Q3	60	100
2,589	14Q10	60	100
2,760	15B	12	30
2,760	15Q3	42	100
2,760	15Q10	42	100
1,501	31B	51	100
1,501	31Z3	340	1,000 *
2,018	32B	31	100
2,018	32Z3	270	1,000 *
2,381	33B	25	100
2,381	33Z3	205	500 *
2,589	34B	15	30
2,589	34P3	15	30
2,589	34Q3	100	300
2,589	34P10	15	30
2,589	34Q10	100	300
2,760	35B	9	30
2,760	35P3	9	30
2,760	35Q3	25	100
2,760	35P10	9	30
2,760	35Q10	25	100
2,943	36B	9	30
2,943	36P3	9	30
2,943	36Q3	22	30
2,943	36P10	9	30
2,943	35Q10	22	30
Shelter	SH-V	1G	5

* Ultradyne S-6; all others Wianeko.

in surface characteristics between the very-dusty Frenchman Flat area and the gravelly, vegetated surface of Area 2c might be expected to affect the results. Without considering this difference, Figure 2.3 shows scaled predictions for Smoky, based on Shots Met and Priscilla. The dynamic pressure curve used for Priscilla is taken from the pretest predictions, since it was concluded that this best represented the general trend of the preliminary results.

In Figure 2.3, there is little to choose between the two sources, and the Line 1 predictions shown in Figure 2.4 represent a reasonable compromise between the two. In this figure,

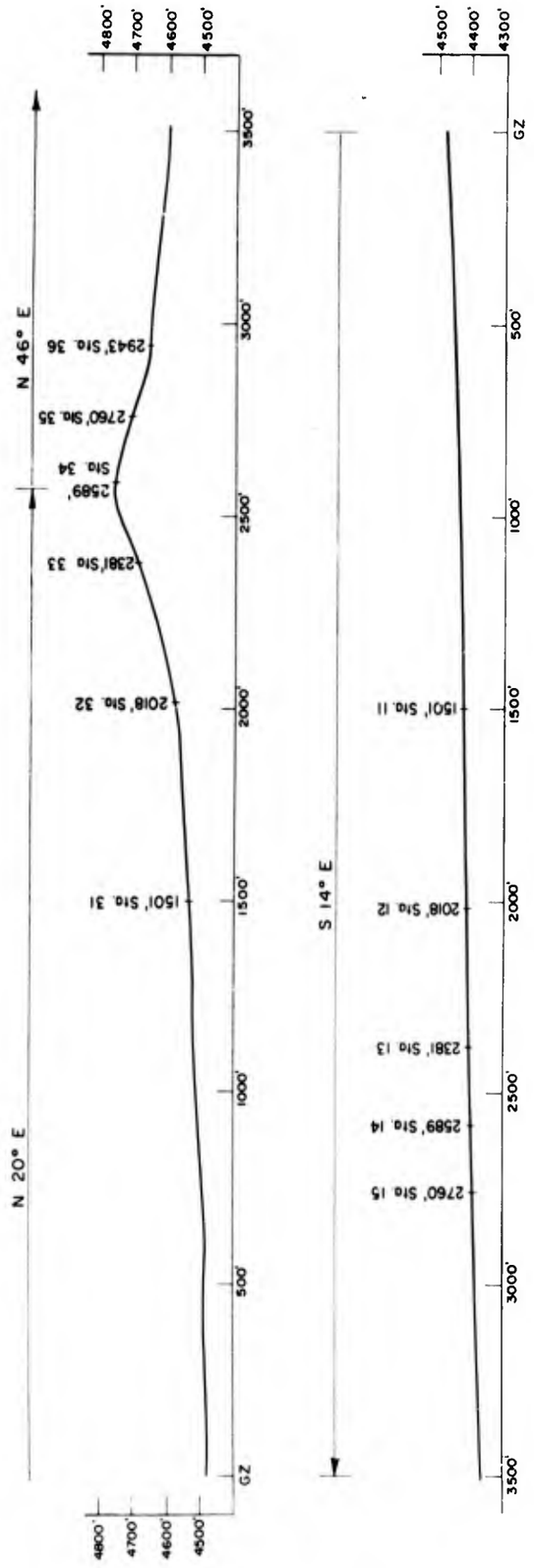

Figure 2.2 Profile of gage lines.

the station locations of interest are indicated by data points. Quantitative predictions taken from these points are shown for each gage channel in Table 2.1. Values for dynamic pressure and overpressure are taken directly from the curves; those for total-head pressure are the sum of the dynamic pressure and overpressure.

2.2.2 Ridge-Line Predictions. The Line 3 predictions are necessarily based on those for Line 1. The problem is one of anticipating the pressure ratios that are appropriate to the slopes, pressure levels, and wave forms at each station.

Overpressure. Figure 2.2 shows that a generally flat slope of about 2 degrees from horizontal extends from ground zero to a point beyond Station 31. This slope increases

TABLE 2.2 COMPARISON OF SHOT DATA

Shot	Yield	HOB	P_o	Scale Factor		HOB	Relative Scale Factor*	
				Distance	Pressure	A-scaled	Distance	Pressure
	kt	feet	mb			feet		
Smoky	45	700	835	3.79	0.825	185	1.0	1
Met	22	400	884	2.93	0.873	136	0.774	1.06
Priscilla	39	700	887	3.54	0.876	198	0.935	1.06

* Relative to Smoky.

gradually; at Station 33 the slope is about 22 degrees, with Station 32 located near the point of maximum inflection. Station 34 is on the crest of the ridge, and Station 35 is at a point where the negative slope is about 20 degrees.

At the first station and at the top of the ridge, the pressure ratio should be 1.0, since no slope effect should be present. At Station 33, the pressure ratio is expected to be about 1.35 (see Section 1.3), and at Station 35, about 0.75. At Stations 32 and 36, intermediate values are expected. The pressures predicted for Line 1, multiplied by these values, are shown as the predicted values for Line 3 in Figure 2.4 and in Table 2.1.

These predictions ignore the possible effects of increased thermal radiation impinging on the front slope. It may be argued that the extra thermal flux will cause an abnormal depression of overpressure, beyond that normally seen in a precursor. The mechanism of this effect, which is not well understood, can be safely ignored for prediction purposes.

Dynamic Pressure. Dynamic pressures on Line 1 can be predicted with some degree of confidence. On Line 3, these dynamic pressures may be modified by the slopes by two mechanisms, thermal and mechanical. As an example of probable thermal effects, Station 13 (2,381 feet ground range on Line 1) is in the region of Type 3 wave forms of overpressure (see appendix), a region near the end of active precursor effects. Station 33, on Line 3, at the same ground range, is on a 22-degree slope at an elevation of about 195 feet above ground zero, 505 feet below burst height. Extending the plane of the slope, this is as if it were at a ground range of 2,011 feet from a 1,360-foot-high burst, definitely in the region of Type 1 wave forms. For thermal reasons, then, the precursor should be enhanced at this station, with the possibility of a near-shock wave front and higher-than-normal dynamic pressures.

On the falling slope, thermal effects will be less than normal, but they are already fairly unimportant. The only thermal effect of the falling slope should be an accelerated cleanup of Types 4 and 5 wave forms.

The mechanical effects of the slopes on dynamic pressures are even more difficult

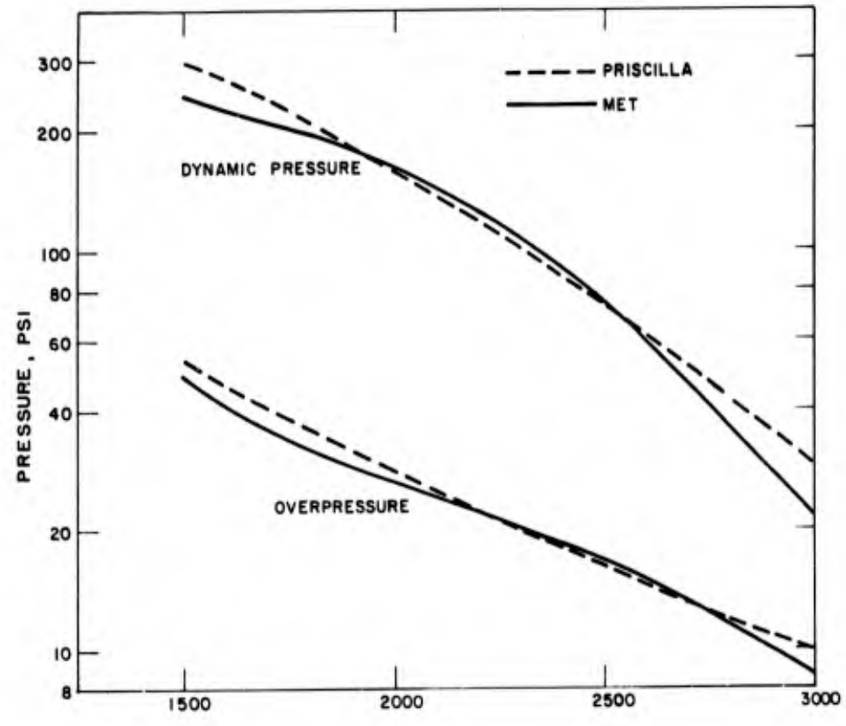

Figure 2.3 Met and Priscilla results, scaled to Smoky.

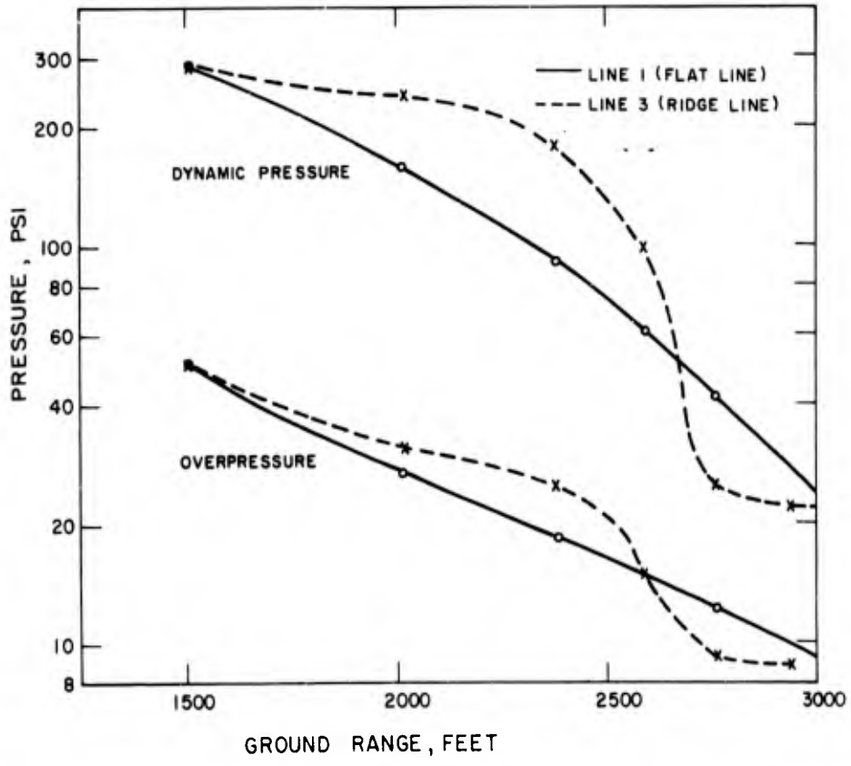

Figure 2.4 Smoky predictions.

to estimate. Considering first an applied shock wave, there is no good reason to believe that the increased overpressures in the spikes observed experimentally are accompanied by a corresponding increase in dynamic pressure. On the contrary, dynamic pressures may very well be decreased. The application of Bernoulli relations would call for such a decrease to accompany an increase of overpressure, as would observations of decreased propagation velocity on front slopes. It can only be assumed that similar effects will prevail with the nonshock, precursor input wave forms expected.

At the upper (convex) portions of the front slope and on the ridge, the mechanical effects should, by analogy to an orifice, cause an increase in particle velocity and dynamic pressure. Similarly, mechanical effects should cause a decrease in dynamic pressure on the back slopes.

In summary, the net thermal plus mechanical effects should cause some increase in dynamic pressure on the front slopes and at the ridge, followed by a pronounced decrease on the steeper portions of the back slope.

For range-setting purposes, it was considered safest to err in the direction of extreme dynamic pressure ratios, since the direction of change from normal seemed reasonably well established. Without further defense of the choices, pressure ratios for dynamic pressures were estimated as follows:

Station	Pressure Ratios
31	1.0
32	1.5
33	2.0
34	1.6
35	0.6
36	0.8

These values were used to derive the predictions of dynamic pressure shown in Figure 1.4 and Table 2.1.

Chapter 3

INSTRUMENTATION

3.1 SHOT PARTICIPATION

Project 1.8c participated in Shot Smoky. The estimated yield at the time of writing of this report was 48 kt. Other parameters for this shot are given in the technical summary report, ITR-1445.

3.2 CENTRAL STATION

All channels of instrumentation were essentially identical to those used in previous operations (Reference 5). Wiancko balanced variable-reluctance pressure transducers or Ultradyne variable-reluctance pressure transducers were connected through modified Wiancko equipment to Willian J. Miller Corporation oscillograph recorders. Provisions were included for applying automatically a synthetic calibrating signal to each channel immediately prior to zero time for purposes of comparison of the final deflection on the record with the deflection produced by the same signal at the time of calibration. A highly accurate timing signal of 100 and 1,000 cps was also applied to all recorders simultaneously from a single source, having a time accuracy of better than 10 parts per million. This provided means for accurate time correlation of events on separate records.

The prime power supply for all instruments during the shot was a bank of storage batteries. Suitable converters were used to produce 115 volts for those components requiring this power source. (During testing and set-up, an engine-generated set replaced the batteries and converters.) An individual converter was used for each rectifier power supply, thus minimizing the probability of gross failure due to converter failure.

Thirty-two gage channels were connected to dual recording systems, consisting of two recorders. The dual channels were used to minimize loss of data due to any single recorder failure. Some of these dual channels used galvanometers of widely different sensitivities to provide a wide dynamic range of usable sensitivity.

Instruments were powered at given times before zero time by Edgerton, Germeshausen, and Grier (EG&G) relay circuits, with lock-in relays controlled by a time-delay relay, allowing continued operation for approximately one minute after zero time, even though EG&G relays dropped out sooner. Utmost attention was paid to circuitry and procedures to insure maximum reliability of operation. Dual relay contacts or dual relays were used wherever feasible. A multipen recorder was connected to provide a record of operating time and sequence of various elements so that any failure might be traced to its source in a posttest study.

To minimize the possible damage due to heavy currents flowing at zero time, known as the induction signal, the signal circuit of each gage channel was grounded during zero time. A number of multicontact relays were used, with one contact connected between each signal lead and ground. Circuits were arranged so that these relays were energized at approximately minus 5 seconds and were de-energized after a short delay by the signals from an EG&G blue box mounted above the shelter. This protection system was used successfully during Operations Upshot-Knothole and Teapot.

The recording shelter housed all central-station equipment used for this project. It

was located partly behind a hill to minimize the prompt radiation and the blast effects received by the recording equipment. It was located at about 2,600 feet from ground zero and was buried to a depth sufficient to reduce the integrated radiation dosage within the shelter to below 10 r. This radiation level had been chosen to represent that which would preclude fogging of the recording paper.

3.3 TRANSDUCERS

3.3.1 Blast Gages. For the basic measurement of surface-level overpressure at all stations, Wiancko pressure gages were used, mounted at the center of a 17-inch-diameter cast-aluminum baffle. This baffle was cemented flush with the earth's surface and was held in place with a buried anchor. In each case a location was chosen that was

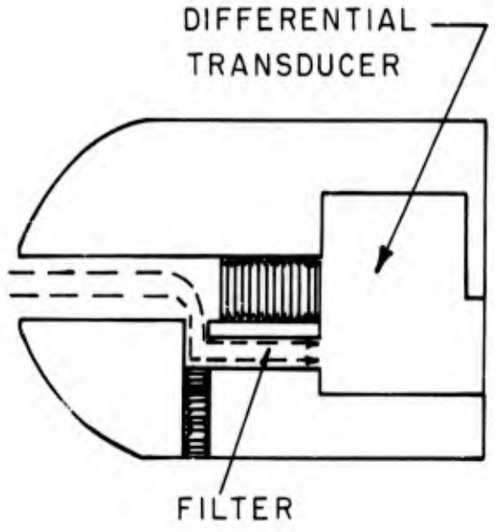

Figure 3.1 Modified head for Sandia-Wiancko pitot-tube gage.

reasonably flat and at a slope representative of the general slope of the terrain at that ground range. Due to the nature of the terrain, these conditions could be met only within a radius of approximately 6 feet of the gage itself in many cases.

3.3.2 Subsonic Pitot-Tube Gage. The pitot-tube gages for measurement of above-ground overpressure and dynamic pressure were a modified form of the Sandia-Wiancko pitot-tube gage used during Operation Teapot (Reference 5). On that operation some of the gages failed to operate satisfactorily during the latter part of the positive phase, because dust entered the gage mechanism itself and, in some cases, was carried into the gaps between the armature and the coil forms. For Operation Plumbbob, the gage design was changed to provide more indirect entry to the gage cavity itself and to allow use of a more-effective filter to remove the dust collection (Figure 3.1). This increased the fill time of the gage cavity but did not appreciably affect the overall response time of the differential gage system, since that is primarily determined by the difference in fill

time of the two cavities. The pressure entry into the second gage used for overpressure was not modified.

The pitot-tube gages were mounted identically to those used during Operation Teapot (Reference 5), since this mount had proved satisfactory on that operation.

3.3.3 Supersonic Total-Head Gage. The Sandia-Wiancko pitot-tube gage described above was designed primarily for use in flows less than Mach 1. The hemispherical shape of the nose of this gage and the location of the side entry ports causes the correction for Mach number to become large at Mach numbers above approximately 0.9. Wind-tunnel calibrations are available up to this Mach number, but use of this gage above these levels requires extrapolation of the correction curve and results in serious probable errors in the reduced data. In addition, the hemispherical nose causes the pitch or yaw correction to be large.

In the original planning for Project 1.3 of Operation Plumbbob (Reference 6), a new gage (Figure 3.2) was designed for use in the supersonic region. This gage is designed

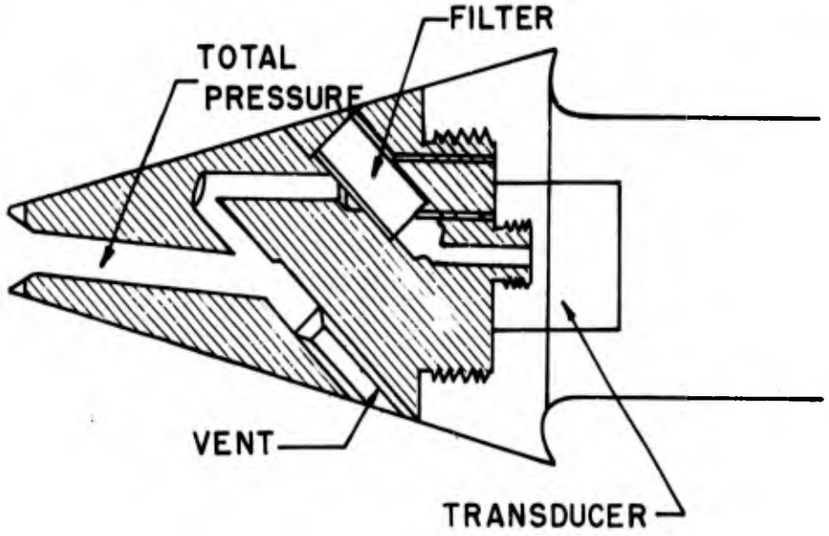

Figure 3.2 SRI supersonic total-head gage.

to measure total-head pressure only, dynamic pressure being derived during data reduction by subtraction of the overpressure measured nearby. The decision to measure total-head pressure was made because use of side ports on supersonic pitot-tube gages requires a very-long space between side ports and the nose of the gage, which would lead to instruments mechanically too weak to withstand the loads expected in the high-pressure region. Elimination of the side ports permitted use of shorter mountings, with resultant improved ruggedness. The design of the gage provided a high degree of resistance to pitch or yaw angle effects, so separate pitch gages were not required.

3.3.4 Gage Towers. The gage towers supporting aboveground gages were, for the post part, moved from the Frenchman Flat area, where they had been used for Shot Priscilla. These towers had successfully withstood high values of dynamic pressure in that shot, so the design was considered satisfactory. In placing the towers for Project 1.8c, each tower was oriented in the vertical plane so as to be perpendicular to the general slope of the terrain in that area. This permitted gages to be mounted essentially

parallel to the local surface. In plan view, the towers were oriented so as to point directly toward ground zero. Typical gage installations on towers are shown in Figures 3.3, 3.4, and 3.5.

3.4 GAGE CODING

A coding system was adopted for identification of channels and recorded traces with their proper gages. Station numbers were assigned to each ground range on each blast line. Station numbers from 10 to 19 were assigned to Line 1, from 31 to 39 to Line 3. Similar ground ranges were indicated by similar second figures. These numbers were used as a first part of the gage code. The second part of the gage code was a letter indicating the type of measurement. In this project, B was used for air blast measured by conventional baffle-mounted gages; P for air blast measured as a side-on component (overpressure) of the

Figure 3.3 Typical gage installation, front slope.

pitot-tube gage; Q for dynamic pressures measured with the subsonic pitot-tube gages; and Z for the total pressure measured by the supersonic total-head gage. A third part of the gage code, where necessary, indicated the height of a gage above the surface in feet. Typical gage code numbers then would be: 11B, a blast gage at the first station on Line 1, zero level; 34Q10, a dynamic pressure gage at the fourth station on Line 3, 10 foot height.

3.5 INSTRUMENT RESPONSE

Response time of the pressure-gage recording system was determined by the characteristics of the recording galvanometers used. The (nominal) 300-cps galvanometers had an undamped frequency of from 315 to 350 cps and were damped to have an overshoot of approx-

Figure 3.4 Typical gage installation, top of ridge.

Figure 3.5 Typical gage installation, back slope.

imately 7.5 percent. This corresponds to a damping factor of approximately 0.65 critical and provides a nominal rise time (to 90 percent of final amplitude) of 1.3 msec. The nominal 200-cps galvanometers had an actual undamped natural frequency of from 200 to 230 cps and were similarly damped, giving a nominal rise time of approximately 1.8 msec. Since the rise time of the Wiancko transducer, when properly adjusted, was appreciably smaller than either of these figures, it does not enter into the characteristics of the final records.

The Wiancko gage system is basically flat down to steady-state conditions. To avoid drift due to temperature changes or changes in ambient pressure, the lower-range gages, are provided with a bleed plug in the gage casing. Thus, any pressure difference between the inside and outside of the case is equalized over a period of time. The time constant of this bleed plug was adjusted to a minimum of 30 seconds so that it would have no effect on the recording of a blast wave of normal duration. As a consequence, the low-frequency response of the gage system may be considered as completely flat.

3.6 CALIBRATION

Each pressure gage was calibrated in the field by the application of several values of static pressure after the gage had been installed in its final location and connected to its associated equipment. After the shot, a postshot calibration was performed on all possible gages to check stability of the system.

In the calibration procedure, several pressures, ranging from zero to well above the expected peak, were applied to the gage in sequence. The galvanometer deflection was noted and recorded for each pressure. In addition, the deflection caused by an artificial signal injected into the gage circuit was recorded. From the former deflection, a calibration curve of deflection versus pressure was constructed; the latter deflection served to correct for any changes of sensitivity in the recording system between the calibration and the final tests, since an identical signal was injected on the final record about 10 seconds before zero time.

Chapter 4

OPERATIONS

Field operations in preparation for this project were partly concurrent with and were performed by the same personnel as those for Project 26.4a, although at all times Project 1.8c was given priority. There were several occasions for delay imposed by outside circumstances, and at these times personnel were shifted to work on Project 26.4a.

The field crew arrived at NTS for this project between 26 and 30 July 1957. The recording shelter, which was being moved from area T 7-3, had not yet been installed, but contractor's work was proceeding on towers and cable trenches.

Fallout from Shot Diablo (on July 15) left a radiation level of up to 50 mr/hr in the area, which impeded the operations through the entire period. The shelter was installed on 3 August, and instruments were installed on 5 August.

The nature of the terrain made it impossible to cut cable trenches to all gage stations. The approximate extent of the trenching installed is shown in the dotted lines of Figure 2.1. Cables to Stations 35, 34, and 33 were laid, from near Station 35, on a layer of sandbags and covered with another such layer to protect them from thermal radiation, blast, and missiles. All trenching was completed and cables laid by August 16. Calibration was completed by 20 August.

The shot, originally scheduled for 19 August, was postponed on about 13 August and when Shot Shasta was fired on 18 August, a date of 28 August was set for Shot Smoky. Weather delays occurred for three successive days, but the shelter was checked and closed on the night of 30 August and the shot was fired on 31 August. Radiation conditions prohibited early recovery, but the shelter was opened and records were recovered on 2 September.

Chapter 5
RESULTS

5.1 INSTRUMENT PERFORMANCE

Of the total of 33 electronic recording channels, 30 produced usable records, with the possibility that one more may be found usable after careful reading and examination. Two channels, 12Z3 and 33Z3, were definitely lost, apparently due to electrical disturbances occurring at or shortly after zero time. Considerable disturbance and noise appeared on most of the channels in the first 300 msec, but these largely disappeared before the first blast-wave arrivals. The cause of this noise was not determined immediately; induction signal disturbance was severe in spite of the protective measures taken, but the noise in question appeared to be due to intermittent shorting of the gage cables, although it began long before the blast wave reached the closest gage cable. This observation would indicate that the effect was associated with direct radiation, possibly ionization of the cable insulation by prompt gamma radiation. The validity of this explanation is increased by the facts that all cable trenches were relatively shallow and that the cables to Station 33, particularly, were only covered by a layer of sandbags. At later times, 11 channels suffered permanent cable breaks, but these occurred well after the completion of the pressure-time positive phase.

The accelerometer installed in the instrument shelter recorded a maximum vertical acceleration of 0.6 g. There was no apparent effect on the pressure-time traces due to this acceleration. No film fogging was observed on the developed records.

Preliminary reports from the two stations used for shock photography are that only one camera station gave usable data.

5.2 DATA REDUCTION

Arrival times, peak deflections, and times of peak were read from the original records. All readings were taken manually with simple scales, and computations were made with a slide rule, using the field calibration data modified for any change of overall sensitivity by the ratio of the auto-cal signals to the field calibration signals. (This ratio usually differed from unity by not more than 4 percent.)

Each record was traced to separate it from others for examination of wave-form characteristics and for editing out noises that were obviously spurious. After such editing, peak deflections were rechecked for validity.

The preliminary data presented in this report may be changed materially when subjected to complete data-reduction procedures. No attempt is made in this preliminary report to correct the dynamic pressure measurements for Mach number or pitch angle.

5.3 GAGE RECORDS

Figures 5.1 through 5.5 present the tracings of the pressure-time records obtained on this project. The records represent the raw data and have been edited only as described above. No attempt has been made to normalize the records to a common time or pressure scale. Included on the figures are the times of arrival and the designation of peak pressure.

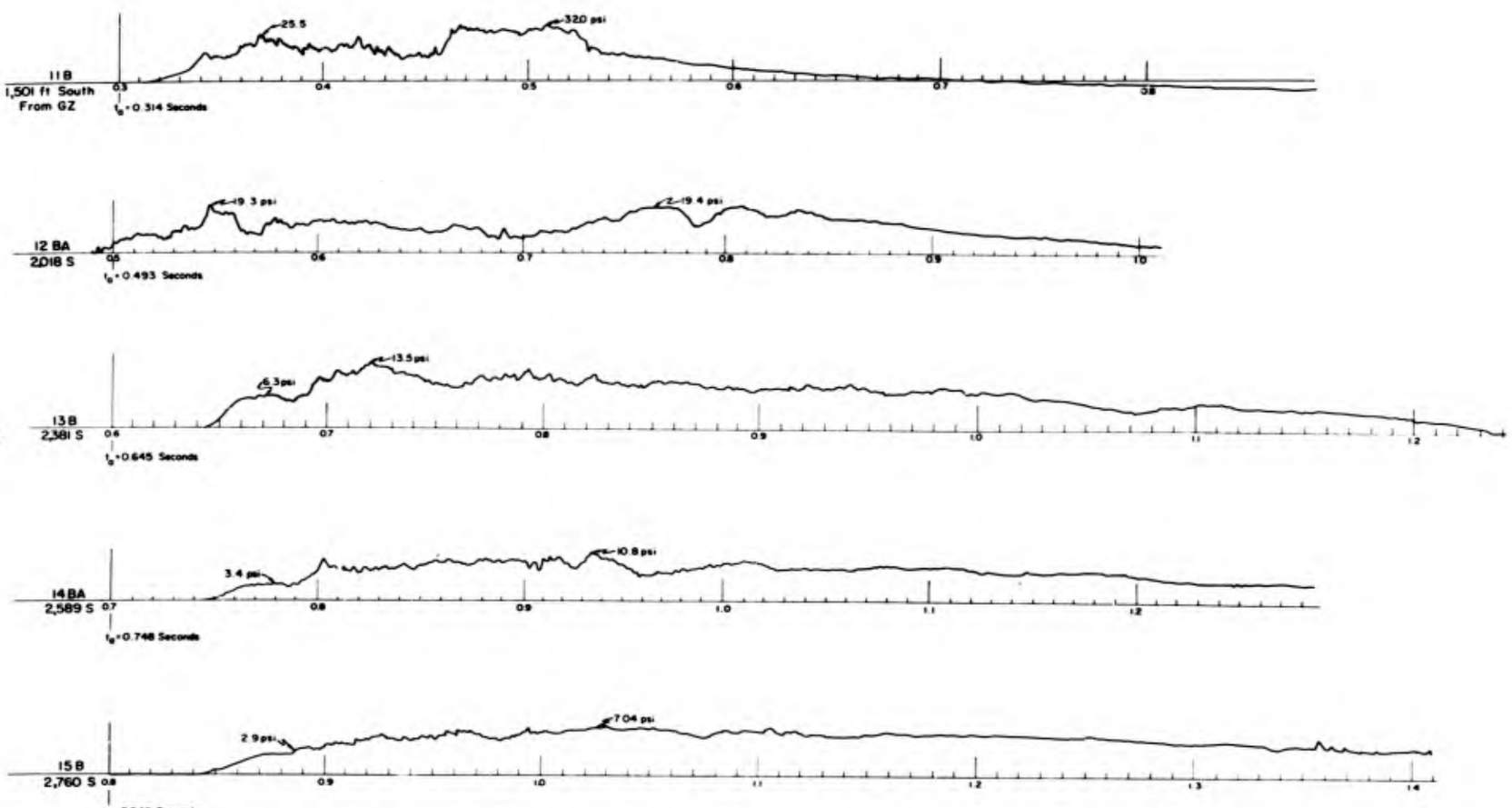

Figure 5.1 Surface-level overpressure, Line 1.

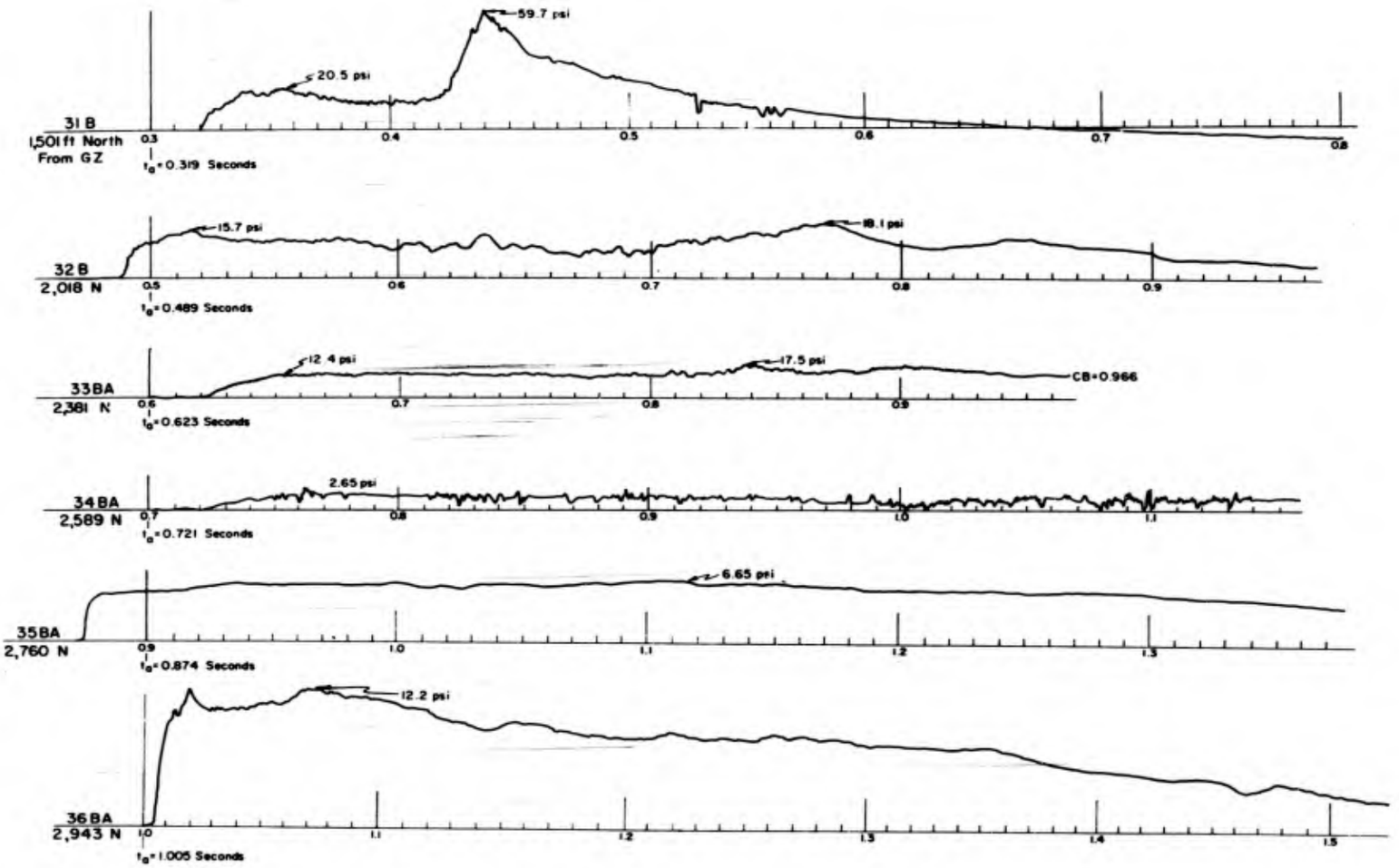

Figure 5.2 Surface level overpressure, Line 3.

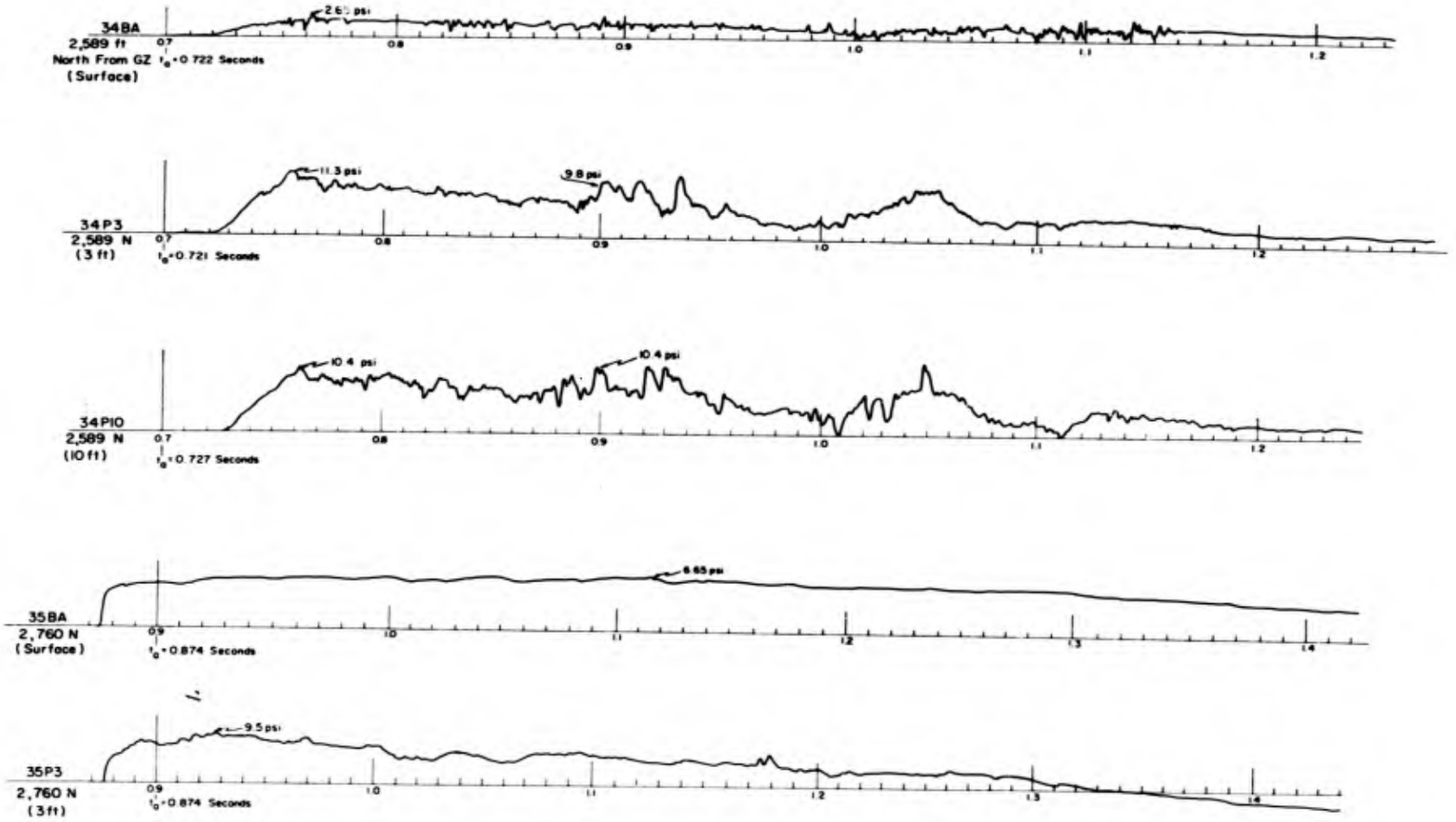

Figure 5.3 Overpressures at surface, 3-foot, and 10-foot levels, Line 3.

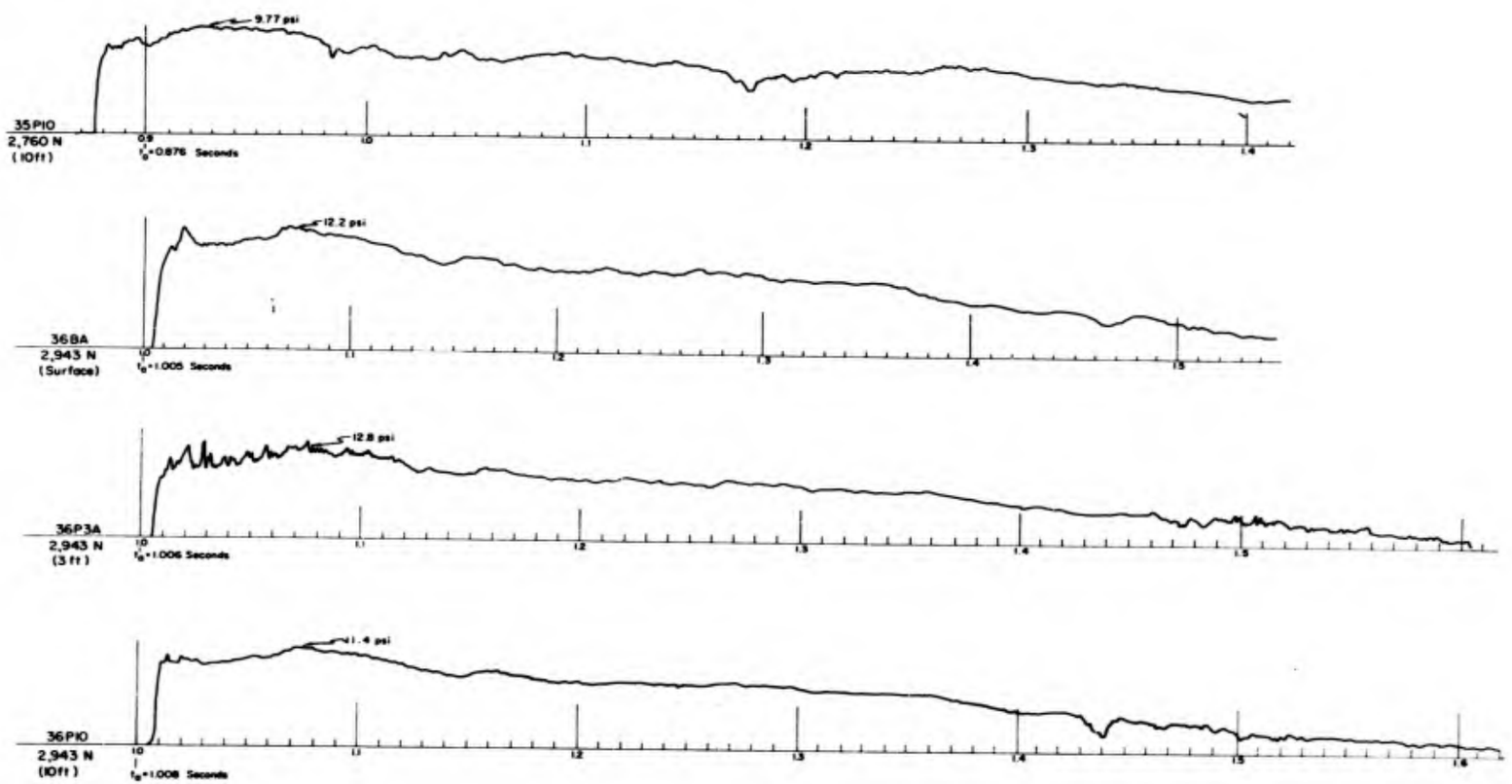

Figure 5.3 Continued.

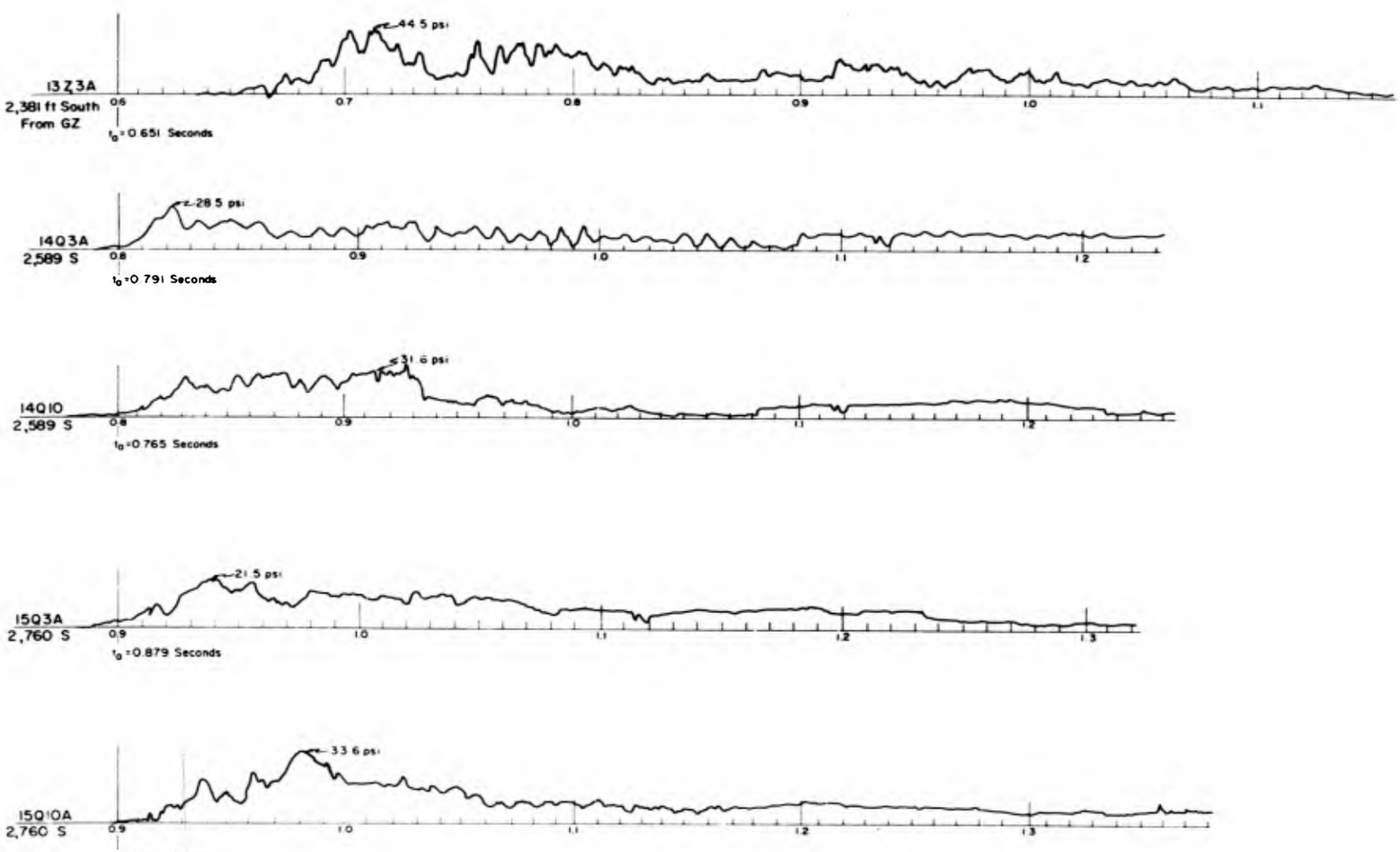

Figure 5.4 Total-head pressure and pitot-tube dynamic pressure, Line 1.

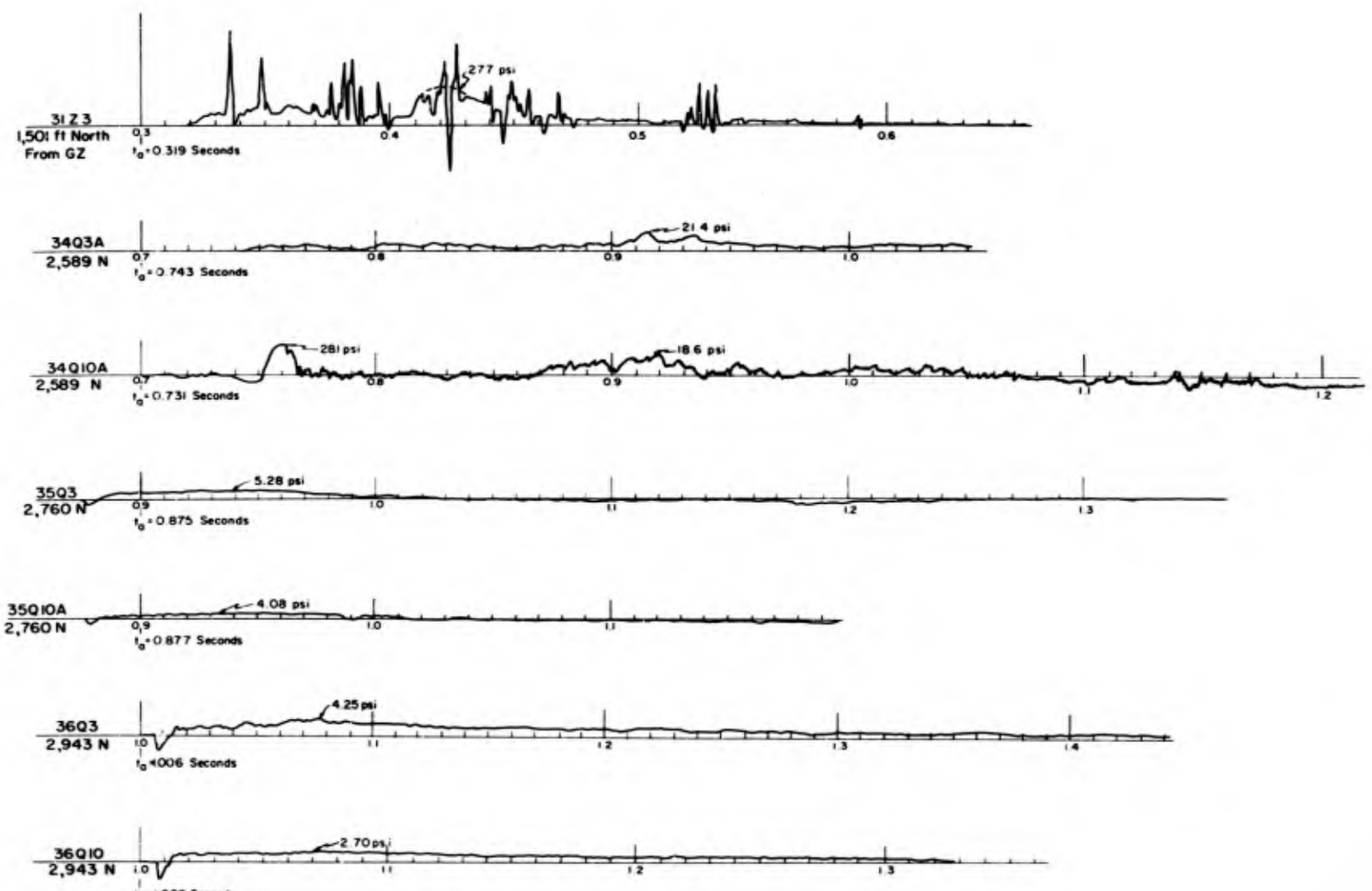

Figure 5.5 Total-head pressure and pitot-tube dynamic pressure, Line 3. (No record at 3,223 and 3,323 feet north.)

The records of surface-level overpressure versus time, included in Figures 5.1 and 5.2, indicate that a well-established precursor wave progressed out from ground zero over Lines 1 and 3. The records have the characteristic hashy appearance of precursor pressure-time measurements. Figure 5.3 shows the results obtained from the static-overpressure

TABLE 5.1 OVERPRESSURE

Gage	Ground Range	Surface Elevation*	Gage Height	Arrival Time	Initial Precursor Pressure	Maximum Pressure	Time of Maximum	Wave Form Type †
11B	1,501	−58	0	0.314	25.5	32.0	0.508	1+
12B	2,018	−71	0	0.493	19.3	19.4	0.770	1+ or 2−
13B	2,381	−85	0	0.644	6.3	13.5	0.720	1+ or 2−
14B	2,589	−90	0	0.748	3.4	10.8	0.930	1+ or 2−
15B	2,760	−95	0	0.841	2.9	7.04	1.030	3
31B	1,501	+53	0	0.319	20.5	59.7	0.440	1
32B	2.018	+63	0	0.489	15.7	18.1	0.768	1+
33B	2,381	+195	0	0.623	12.4	17.5	0.838	3
34B	2,589	+280	0	0.721	—	2.65	0.765	3
34P3	2,589	—	3	0.721	—	11.3	0.757	2 or 3
34P10	2,589	—	10	0.727	—	10.4	0.762	2 or 3
35B	2,760	+220	0	0.874	—	6.65	1.102	4
35P3	2,760	—	3	0.874	—	9.50	0.927	3
35P10	2,760	—	10	0.876	—	9.77	0.930	3
36B	2,943	+170	0	1.005	—	12.2	1.071	3
36P3	2,943	—	3	1.006	—	12.8	1.075	3
36P10	2,943	—	10	1.008	—	11.4	1.070	3

* Referenced to ground zero approximate.

† For discussion and illustration of wave-form types see the appendix to this report and References 5 and 6.

gages mounted in the pitot-tube configuration 3 feet and 10 feet above ground on the top and back slope of the ridge. In general, the records of aboveground pressure versus time appear to be similar to corresponding surface-level records.

Figures 5.4 and 5.5 present the total-head and pitot-tube dynamic-pressure measurements from Lines 1 and 3, respectively. Generally, the records are similar to those

TABLE 5.2 DYNAMIC PRESSURE

Gage	Ground Range	Gage Height	Arrival Time	Maximum Total-Head Pressure	Maximum Dynamic Pressure	Time of Maximum
	feet	feet	sec	psi	psi	sec
12Z3	2,018	3	NR	NR	NR	NR
13Z3	2,381	3	0.651	44.5	33.4*	0.713
14Q3	2,589	3	0.791	—	28.5	0.824
14Q10	2,589	10	0.765	—	31.6	0.917
15Q3	2,760	3	0.879	—	21.1	0.943
15Q10	2,760	10	0.896	—	33.6	0.981
31Z3	1,501	3	0.319	277	250 *	0.423
32Z3	2,018	3	NR	NR	NR	NR
33Z3	2,381	3	NR	NR	NR	NR
34Q3	2,589	3	0.743	—	21.4	0.914
34Q10	2,589	10	0.731	—	28.1	0.759
35Q3	2,760	3	0.875	—	5.28	0.935
35Q10	2,760	10	0.877	—	4.08	0.930
36Q3	2,943	3	1.006	—	4.25	1.078
36Q10	2,943	10	1.008	—	2.70	1.078

* These figures obtained by subtracting the instantaneous reading of surface-level overpressure from the maximum total-head pressure.

obtained during previous precursor-forming shots. It is believed that the excessive disturbance on the 31Z3 record (Figure 5.5) resulted from electrical disturbances, rather than actual pressure variations at the gage inlet.

Tables 5.1 and 5.2 present a summary of the Project 1.8c data. The tabulated data are as-read and must be considered as preliminary. Where dual channels were used to record identical measurements, an average of the two results is reported (except where one of the deflections was so small as to make its accuracy questionable).

Chapter 6
DISCUSSION

No effort is made in this report to derive any rigorous relationship between the phenomena observed and the geometry of the terrain or the pressure levels applied. The irregular, asymmetrical nature of the terrain and the limited number of measurement points prohibits any such attempt, particularly in an interim report. Rather, an attempt is made to observe the trends and general magnitudes of the effects and to compare them with the observed and derived effects of slopes on low-pressure shock waves.

6.1 WAVE-FORM CLASSIFICATION

Before attempting to discuss in detail the data obtained on Project 1.8c, the overpressure-time records will be examined on a purely qualitative basis. A detailed description of the SRI wave-form classification system is presented in Reference 5; however, the classifications are summarized in the appendix to this report. Table 5.1 presents the assigned classifications for the overpressure records obtained by this project.

Project 1.8c surface-overpressure wave-form types are plotted in Figure 6.1, a height-of-burst chart for overpressure wave forms. In general, aboveground wave forms are similar. The regions where the various types of wave form would be expected to appear (on precursor-forming shots) are labeled in the figure (Reference 5).

Initially, it should be stated that the pressure-time wave forms obtained on this project were generally not pure forms, i.e., most of the forms could not be placed unreservedly into a single classification. Nevertheless, looking at Figure 6.1 (and referring to the pressure-time records of Figures 5.1 through 5.3), it is evident that wave forms along the two blast lines were quite different.

It was expected that the first stations on each line would give about the same results; that this was apparently not so, hints at some asymmetry in the blast wave as it traveled out from burst point. Actually, the 31B record is a pure Type 1, whereas the control-line record (11B) shows significant deviations from the pure form.

At longer ground ranges, the wave forms indicate that the precursor dissipated more rapidly over the ridge line than over the flat line. These differences in wave form along the two lines are not severe, and due to the apparent asymmetry, it would be unwise to draw definite conclusions from such limited data.

No attempt will be made in this report to classify the wave forms associated with the dynamic-pressure measurements.

6.2 OVERPRESSURE

Peak values of observed overpressure are tabulated in Table 5.1 and are plotted against ground range in Figure 6.2. In the study of these data, reference should be made to the tracings of the pressure-time records of Figures 5.1 through 5.3, since they clarify some of the variations evident in the peak readings. In Figure 6.2, the solid line shows the variation of surface-level peak overpressure with ground range as measured on Line

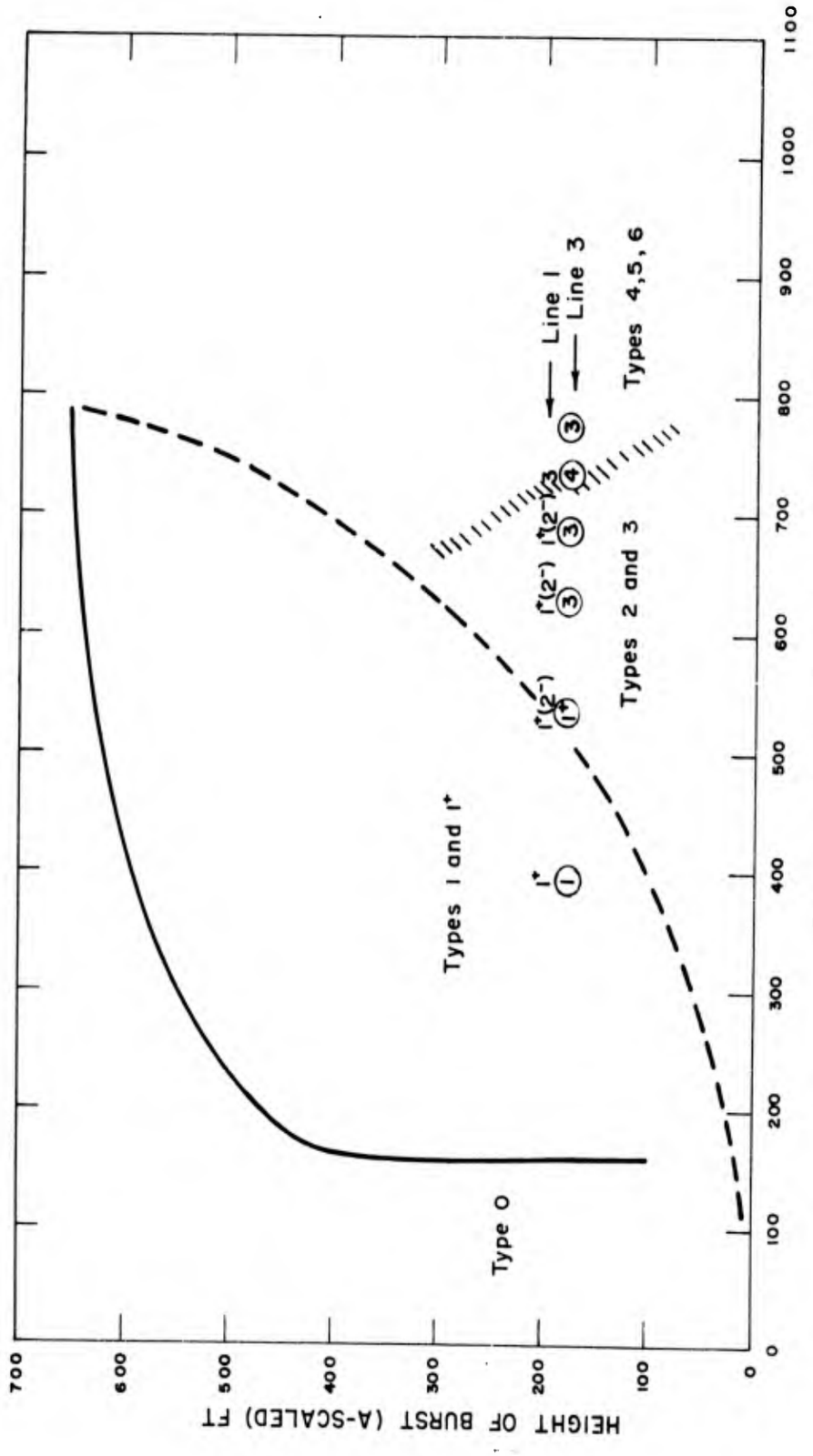

Figure 6.1 Height of burst for surface-level-overpressure wave forms.

1, the flat control line. The drop in pressure at 2,760 feet is unusual, but there is at present no reason to suspect the validity of this point. The regularity of this curve is in sharp contrast to that for Line 3, shown as a broken curve. Point-by-point examination of the data is necessary to interpret these variations.

At 1,501 feet,the Line 3 peak pressure was almost twice that of the flat line; although both stations were in flat terrain, the wave forms (11B and 31B, Figures 5.1 and 5.2) show a pronounced difference. Gage Record 31B is a typical Type 1 wave form, with the late peak value over twice that of the first pressure rise. Record 11B is somewhat atypical; it resembles a Type 2 form with the late peak, only slightly greater than the first peak, occurring somewhat later than that of 31B, although the 11B first arrival is slightly earlier. These features indicate that the precursor was more fully developed at this ground range on the flat line than on the ridge lines (see Section 6.1). At this state of precursor development, peak pressure is a very sensitive function of wave form.

At 2,018 feet, the peak pressures on the two lines were essentially equal, in spite of the fact that Station 32 on the ridge line was at the foot of the front slope. From previous experience with shock waves, a sharp spike might have been expected at the beginning of Record 32B. Its absence confirms the prediction of Section 1.3 that the slow rise of a precursor would prohibit this effect. If there was any increase in average pressure due to the slope, it has been masked in the record by other variations. (A difference may be evident when the curves are integrated to obtain total positive impulse.)

At 2,381 feet, the ridge-line peak overpressure was again higher than that of the flat line. The peak-pressure ratio is 1.3, very close to that predicted. It appears that here the rising slope did affect the overpressure meaningfully.

At 2,589 feet, the top of the ridge on Line 3, the peak value of Record 34B drops very markedly to about 25 percent of that of 14B, an effect which was not predicted but which might be expected in a sharply convex region where air-flow velocities are high.

The reduction of surface-level overpressure was greatly minimized, if present at all, at 2,760 feet on Line 3, a location near the middle of the back slope. At 2,943 feet, at the foot of the slope, there was again a pressure increase, even greater than the 30-percent increase at Station 33. Gage Record 36B at this station shows the only occurrence of what may be a spike. This, however, is small and cannot definitely be identified as a terrain effect.

Aboveground overpressures were measured at the last three stations on the ridge line and are shown in Figure 5.3, while the data are plotted in Figure 6.2. In contrast to the surface-level measurements, the data shows no reduction of the 3-foot peak pressure at the top of the ridge. There was no important difference in the 3-foot and 10-foot peak overpressures.

The terrain contours of Figure 2.1 show that the ridge line crossed the ridge near its end. There had been some concern as to the effects of diffraction around the end of the ridge upon the measurements at Stations 35 and 36. If such had been present to any extent, secondary peaks would be expected on the pressure-time wave forms from these stations. No such secondary peaks are evident.

From the standpoint of maximum overpressure, it is concluded that a ridge of the type studied offers no protection, except very near the surface in the sharply convex regions only. Overpressures are somewhat increased on the front face and near the bottom of the back slope.

6.3 DYNAMIC PRESSURE

Peak values of observed dynamic pressures are tabulated in Table 5.2 and plotted

against ground range in Figure 6.3. Again, in studying these data, reference should be made to the pressure-time records of Figures 5.4 and 5.5.

In Table 5.2, the fifth column lists the total-head pressure measured by these total-head gages that produced records. To reduce the data to approximate dynamic pressure, the corresponding record for surface-level overpressure was read at the time of maximum indicated in the seventh column. This value of overpressure was subtracted from the maximum total-head pressure to obtain the value of maximum dynamic pressure shown in the sixth column. Also in Table 5.2, arrival times shown are by no means as accurate as those for overpressure, due to the difficulty of determining the first departure of the slowly changing pressure-time record. No conclusions can be drawn from these arrival times as to the departures of the blast front from vertical, at least until more precise reading methods are applied.

Referring to Figure 6.3, the failure of Gage 12Z3 limited the data from the flat line to Stations 13, 14, and 15. Over this range, the values for 3-foot dynamic pressures (as read) show a reasonable decay with ground range; also, the 10-foot values are higher, which is in accord with previous experience. However, values for the two 10-foot peak dynamic pressures do not show a decay with increased ground range. There is no evident explanation for this minor anomaly.

The variation of 3- and 10-foot dynamic pressures on the ridge line is shown by the two dashed lines in Figure 6.3. The peak value of 250 psi at 1,501 feet is well documented and reasonable. Gage failures at the next two stations leave the shape of the curve between 1,501 feet and the top of the ridge in doubt. At the ridge top, the measured dynamic pressures were slightly lower than those on the flat line, but not significantly so. Both the wave forms and the ratio of dynamic pressure to overpressure show that precursor effects were still present at this range, to about the same extent on both lines. Also, on the ridge line the 10-foot-level dynamic pressure was higher than at 3 feet, as was the case on the flat line.

At the next station, on the back slope, the peak dynamic pressure dropped markedly below corresponding values on the flat line. The dynamic pressure ratio is about 0.25 at 3 feet, and about 0.12 at 10 feet. The 10-foot-level pressure was here lower than at 3 feet, a reversal of the usual circumstance. These conditions continued at the last station, at the foot of the back slope, where the maximum dynamic pressure continued to decrease, even though peak overpressure increased at this station. The measured values of dynamic pressure at this last station are about equal to the values predicted by Rankine-Hugoniot equations for a clean shock wave with a peak equal to the measured value of overpressure, even though the observed wave forms are not classic.

From the standpoint of dynamic pressure, it is concluded that a ridge of the type studied would offer a real protection to drag-sensitive targets on the back slope and at the foot of this slope. Lack of data prevents any conclusion as to effects on the front slope, but it seems reasonable to suppose that dynamic pressure should be enhanced, although this enhancement, if present, was not observed to hold over to the top of the ridge.

6.4 ARRIVAL TIME AND PROPAGATION VELOCITY

An examination of wave-front arrival times is frequently useful in analysis of precursor effects and other perturbations. Figure 6.4, a plot of the surface-level arrival times listed in Table 6.1, shows the time-distance curves for the two lines studied; the differences are obvious.

At the first station, at 1,501 feet, the earlier arrival was on the flat line, but by only about 5 msec. At 2,018 feet, the ridge-line arrival was earlier, and progressively more

so out to 2,589 feet, the top of the ridge. For about this point, there is a marked change in the slope of the curve, and the value for arrival at the next station is considerably later on the ridge line.

In Figure 6.5, these data are converted into terms of propagation velocity along the surface, corrected for slope (Table 6.1), and plotted against ground range. (The correction for slope does not change the general shape of the curve.) On the flat line, the velocity

TABLE 6.1 WAVE FRONT VELOCITY, SMOKY

Gage	Ground Range	Time of Arrival	Interval Velocity	Average Velocities	Terrain Slope	Velocity Correction for Slope
	feet	sec	fps	fps	degrees	fps
11B	1,501	0.314				
			2,890			
12B	2,018	0.493				
			2,405	2,648		
13B	2,381	0.644				
			2,000	2,203		
14B	2,589	0.748				
			1,840	1,920		
15B	2,760	0.841				
31B	1,501	0.319				
			3,045			3,045
32B	2,018	0.489		2,843	10	2,880
			2,640		12	2,700
33B	2,381	0.623		2,383	20	2,540
			2,125		16	2,210
34B	2,589	0.721		1,621	0	1,621
			1,117		-16	1,160
35B	2,760	0.874		1,257	-20	1,335
			1,396		-15	1,445
36B	2,943	1,005			-10	

decreased gradually with ground range, as is normal. On the ridge line, the first calculated value of velocity is higher than that for Line 1, although the earlier arrival time for the latter shows that at some closer ground range Line 1 velocities were higher. Although the ridge-line velocities did not actually increase on the front slope, they did not decrease as rapidly as those over the flat line, until near the top of the slope. As the ridge was passed, the Line 3 velocity dropped rapidly to approximately sonic velocity, then rose to join or exceed the velocity over the flat line.

The shape of the velocity curves appears to indicate enhanced thermal effects on the front slope (see Section 2.2.2), since the observed high velocity cannot be correlated with the small pressure increase observed on the front slope. The drop in velocity on the back slope was probably a combined effect of diffraction and of minimized thermal effects. Moreover, this low value is consistent with the observed dynamic pressures, since particle velocity must drop to permit a drop in propagation velocity.

6.5 FLAT-LINE COMPARISONS

Although the main objective of this project, namely to determine the effects of terrain variations upon blast waves, has been discussed in detail, it is germane to compare the flat-line data with results obtained previously in Nevada.

For peak surface-level overpressure the comparison is made in Figure 6.6. In this figure the TM 23-200 (Reference 7) curves for the average and poor surface conditions (scaled to Smoky yield and ambient pressure) are shown with the measured flat-line over-

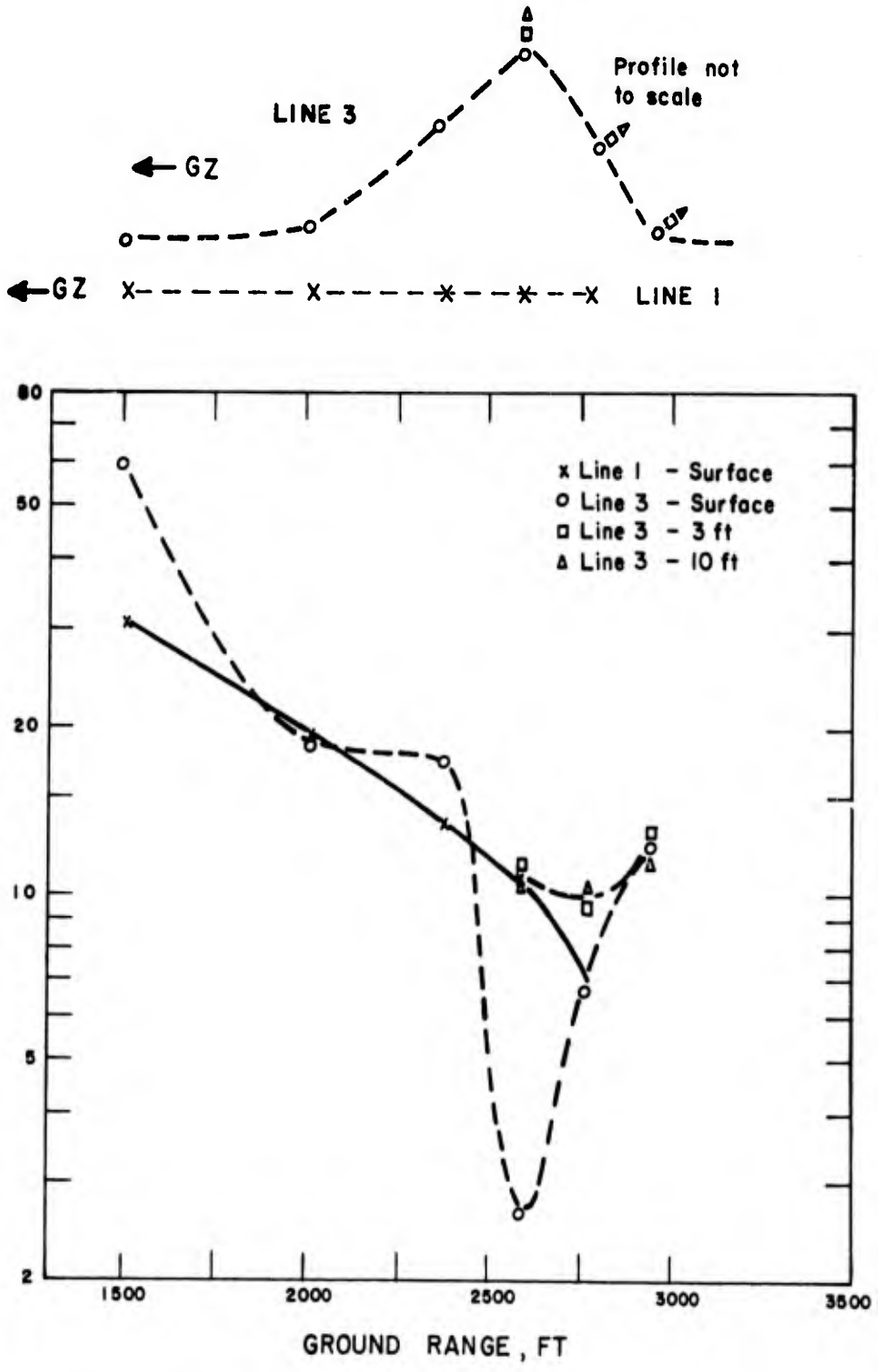

Figure 6.2 Peak overpressure versus ground range.

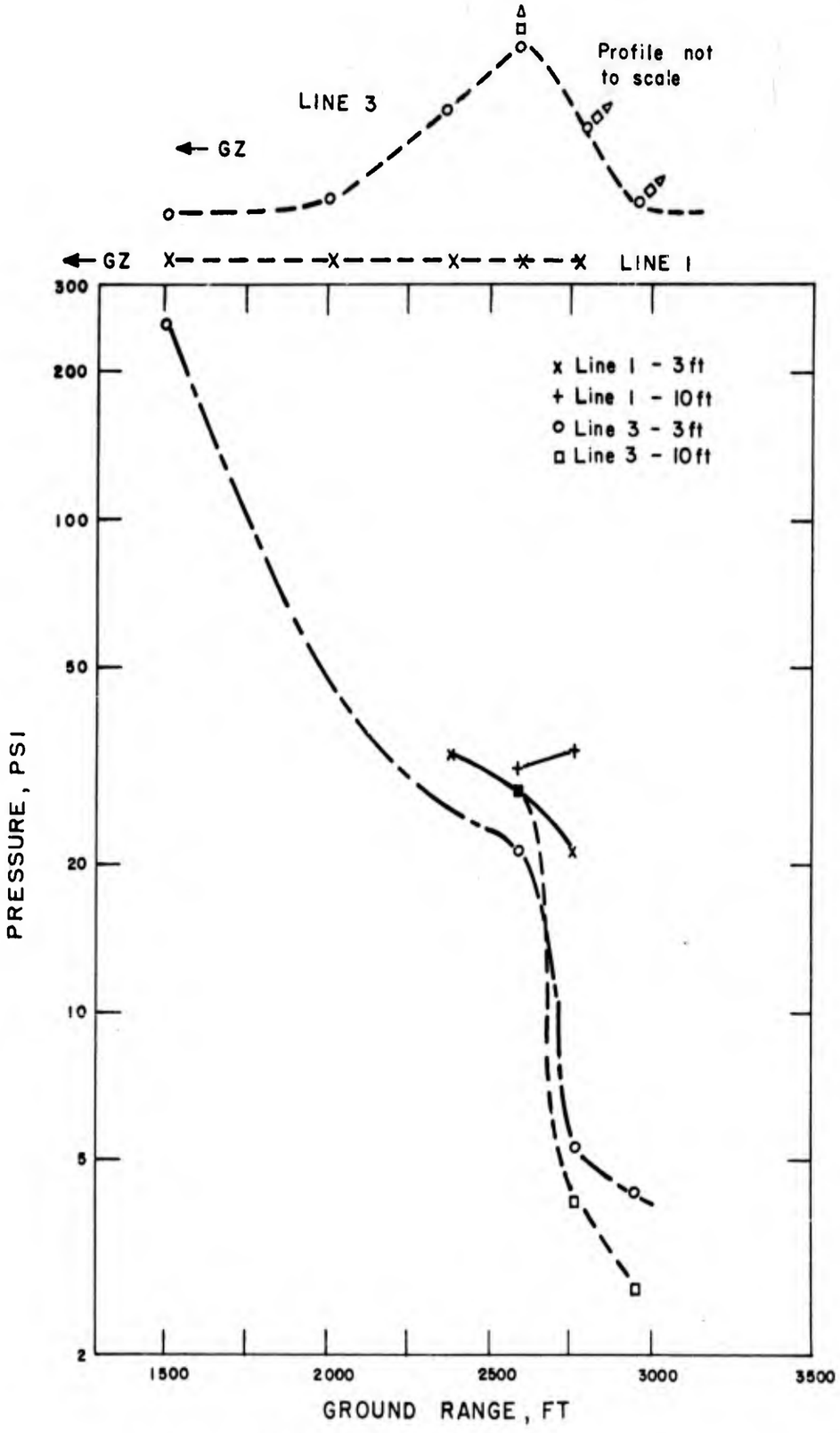

Figure 6.3 Peak dynamic pressure versus ground range.

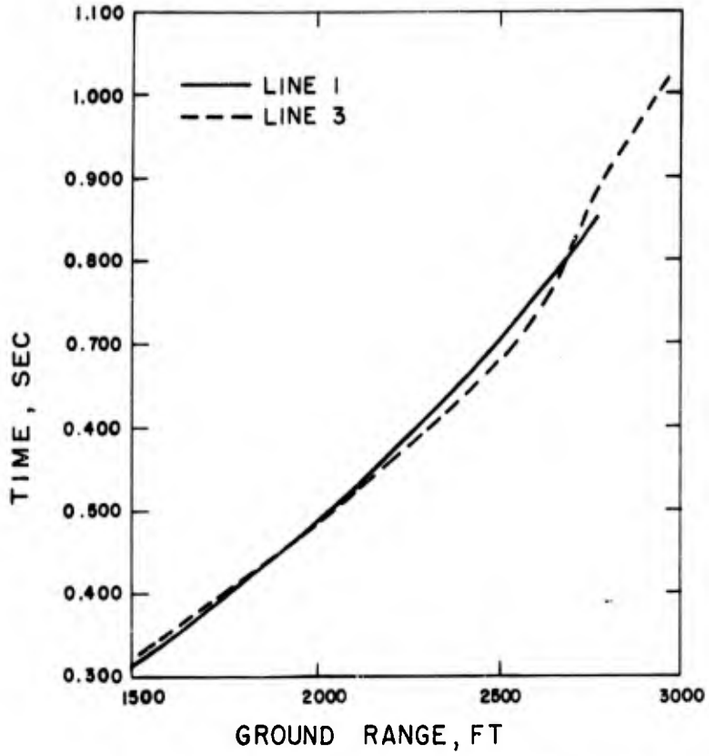

Figure 6.4 Arrival time versus ground range.

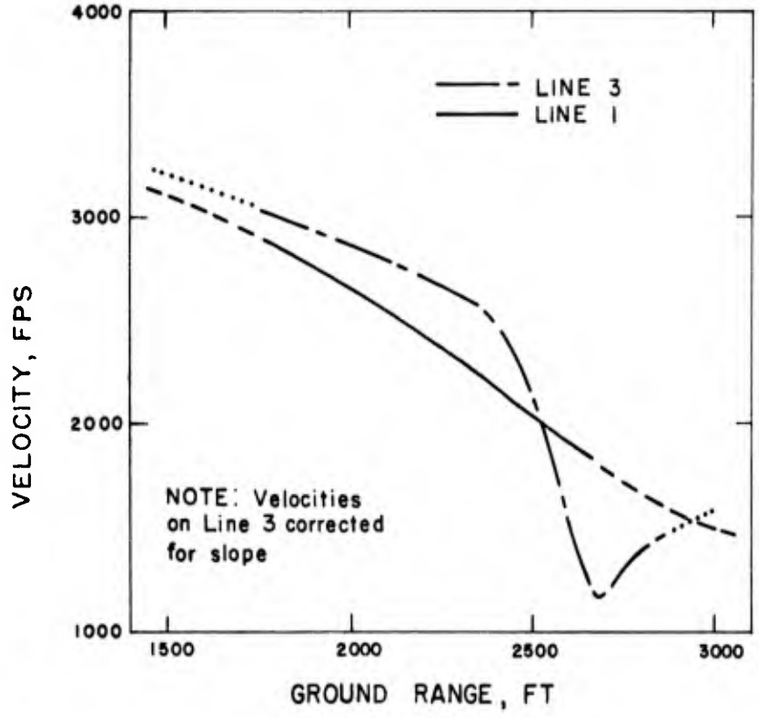

Figure 6.5 Propagation velocity versus ground range.

pressure curve. In general, the Smoky results agree best with the poor surface curve; however, it should be noted that the value for Station 31 on the ridge line is in better agreement with the average surface curve. This result may be due either to a geometrical asymmetry in the blast wave expansion or to a significant difference in surface characteristics along the two blast lines, or both.

Figure 6.7 shows the comparison between the Smoky flat-line dynamic-pressure data and an average curve obtained from the Priscilla and Met data. Where comparisons can be made, the data from previous shots show consistently higher peak dynamic pressures than observed on Smoky. Only at Station 31 on the ridge line (total-head gage) do the data

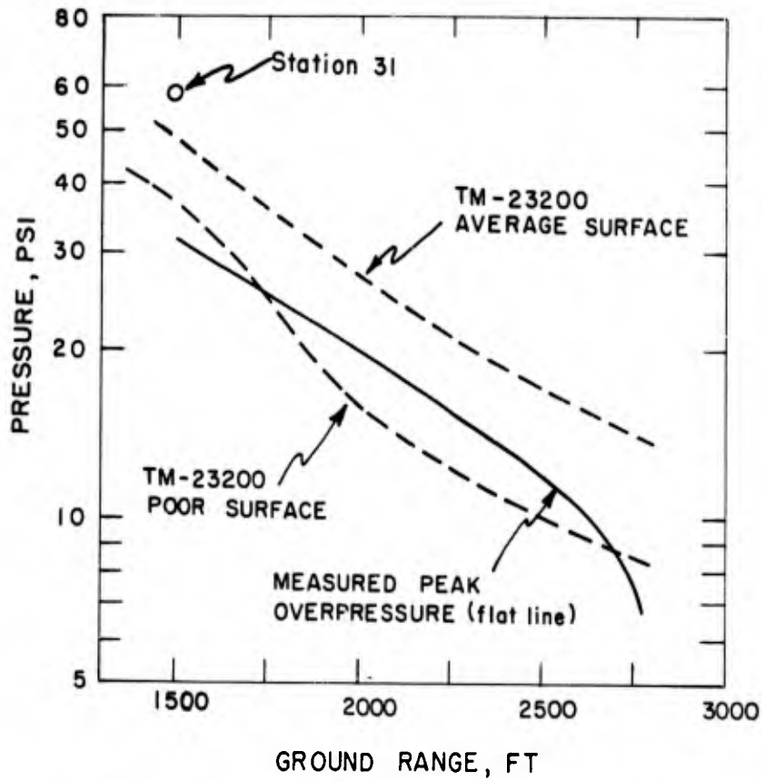

Figure 6.6 Measured peak overpressure compared with TM 23-200.

agree. The Priscilla and Met shots were detonated over a dust-covered Frenchman Flat area, whereas the Smoky area appeared to be more stabilized; an explanation for the discrepancy in measured dynamic pressure might involve these considerations. Further, if it can be assumed that measurements in regions of very-high dynamic pressure (above 100 psi) are not influenced appreciably by dust effects, then the agreement in data at the 1,500-foot range is more understandable.

6.6 INDICATIONS OF ASYMMETRY

It has been noted that the phenomena observed on the two blast lines differed in several respects that are not explained by the profile of the terrain. At the two front stations, the appearance of the overpressure wave forms, the value of the peak overpressure, and the time of arrival indicate that precursor effects were more advanced on Line 1 than on Line 3, even though this condition was reversed at later stations, pre-

sumably due to increased thermal effects on the front slope of Line 3. Two possible explanations for this observation have been advanced: (1) asymmetry of surface conditions in the vicinity of ground zero and (2) asymmetry of shielding introduced immediately underneath the nuclear device for diagnostic purposes.

A considerable area around the base of the tower was leveled and paved with asphalt for access and parking. The center of this area was southeast of the tower. In addition,

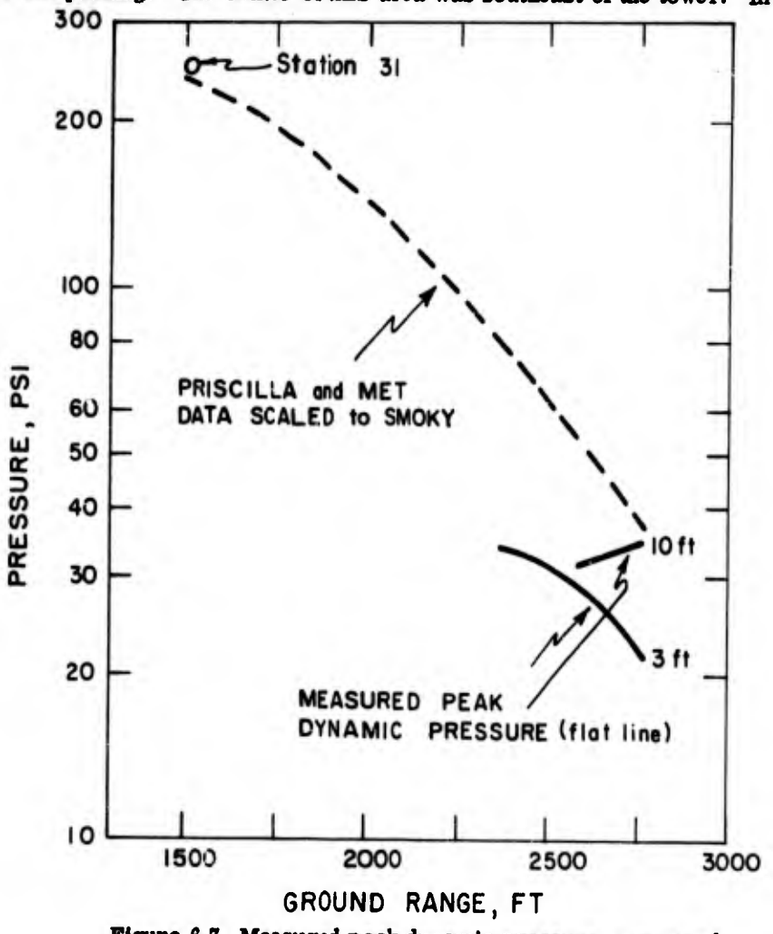

Figure 6.7 Measured peak dynamic pressure compared with Priscilla and Met data.

a paved road led from the tower along a line near Line 1, and several construction projects within 1,500 feet of ground zero in this direction removed the natural vegetation and increased the dustiness of the surface. These conditions may have been the cause of the observed asymmetry.

The shielding underneath the nuclear device has been reported as being centered along a line running north 30 degrees east and concentrated more heavily at the northerly end. From Figure 2.1, it appears that any thermal shielding caused by this local material would be more effective on Line 3 than on Line 1. It would also be more effective at very-short ground ranges. Such thermal shielding could cause the effects noted.

Further study and information on the local shielding are required to evaluate the relative importance of these two conditions and their probable contribution to the asymmetry observed. In any case, it does not seem likely that the general conclusions were importantly affected by this asymmetry or that the conditions described were responsible for the effects discussed in Section 6.5.

Chapter 7

CONCLUSIONS

There is evidence from pressure-versus-time wave forms, peak pressures, and times of arrival, that the Smoky blast wave, as observed at a radius of 1,500 feet, was asymmetrical. This may have been caused by surface conditions or by asymmetry of local shielding installed underneath the device, or both. This situation makes conclusions concerning the effects of the terrain less exact than was hoped, but probably does not affect the general conclusions.

Observations confirm that a precursor formed over both the flat and ridge blast lines; moreover, disturbed blast waves were evident at the farthest gage station on each line. Plots of the wave forms are not pure types and do not lend themselves to definite classification.

Since no significant peaking or pressure spikes are observed from results of the ridge-line overpressure measurements, it is concluded that the precursor-type blast wave prohibited this effect.

For overpressure, a peak-pressure ratio of about 1.3 was observed on the front slope of the ridge and at the foot of the back slope. Also, there is evidence that overpressures (near the surface only) at the ridge top were significantly depressed. Generally, the ridge studied offered no real protection from overpressure.

For dynamic pressure, it is concluded that a ridge of the type studied would offer significant protection to drag-sensitive targets along the back slope and at the foot of the back slope. Although it seems reasonable to suppose that the dynamic pressure would be increased on the front slope, lack of data prevents any definite conclusion on this effect.

Surface-level wave-front-propagation velocities indicate enhanced thermal effects on the front slope of the ridge and a strong diffraction effect as the wave passed over the top of the ridge.

Comparison of Smoky data with those of previous shots shows generally lower-than-predicted values of both peak overpressure and dynamic pressure. Increased thermal absorption and decreased dust loading due to surface conditions may explain these effects.

Appendix

OVERPRESSURE WAVE—FORM CLASSIFICATION

Type	Description of Form	Relation to Previous Type
0	A sharp rise to a double-peaked maximum; peaks close together in time and approximately equal in amplitude.	In its ideal form, it is the classical single-peaked shock wave but is usually recorded as a double-peaked wave.

1	A sharp rise to first low peak followed by either a plateau or a slight decay, then a higher second peak preceding the rapid decay. Time interval between first and second peaks can vary significantly; shock-like rises are evident.	The first low peak indicates the existence of a disturbance which travels faster than the main wave. This type is distinctly nonclassical.

2	Same as Type 1 except that second peak is less than first.	The second peak has decayed to a lower value than the first and has become more rounded and less distinct. Second peak finally disappears.

3	A first large, rounded maximum followed by decay; then a later, usually smaller, second peak. Pressure rises may be slower than for Type 2.	The first peak of Type 2 has developed to become the rounded maximum, while the second peak has decreased in magnitude with respect to the first.

4 A long-rise-time flat-topped form which exhibits a long decay time and much hash.

The relatively sharp pressure rise of Type 3 has been replaced by a slow rise and the second peak has disappeared.

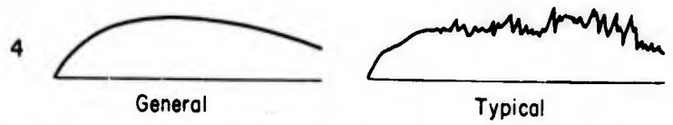

5 A pressure rise to a rounded plateau which is followed by a slow rise to a second, higher peak.

The single-peaked hashy form of Type 4 seems to develop a compression-type second peak, which may be the first indication of the return of the main wave.

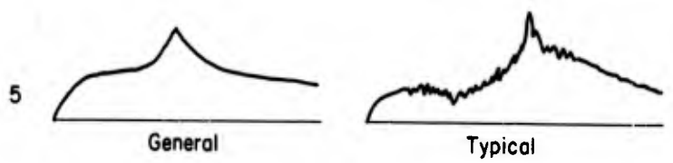

6 A clear-cut double peak form with a rise to a plateau which slopes upward, then a shock rise to a peak.

This is clearly a cleaned-up Type 5, with the compression-type second peaks becoming shocks.

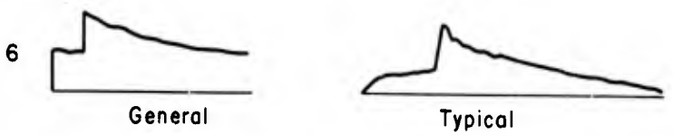

7 A shock rise to a peak followed by either a slight gentle rise, a plateau, or in later examples, a slow decay.

The second peak of Type 6 has overtaken the first peak, resulting in a wave form which is close to classic; sharp, single peak is not evident.

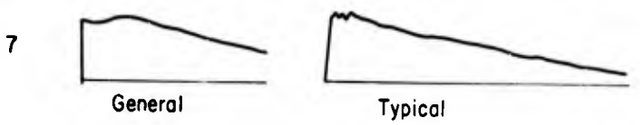

7R Refers to Type 7 in region of regular reflection where a second (reflected) shock front is evident.

Second rise due to reflected wave.

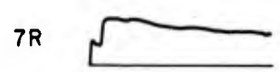

8 A classical wave form.

Sharp single-peaked form, followed by classic decay.

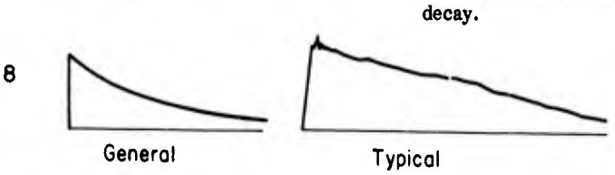

8R Refers to classical wave form in region of regular reflection.

Second rise due to reflected wave.

REFERENCES

1. Merritt, M. L.; "Air Shock Pressures as Affected by Hills and Dales"; Operation Tumbler–Snapper, WT–502; Sandia Corporation, Albuquerque, New Mexico; Confidential Restricted Data.

2. Merritt, M. L.; "Air Shock Pressures as Affected by Hills and Dales"; Operation Upshot–Knothole, WT–713; Sandia Corporation, Albuquerque, New Mexico; Secret Restricted Data.

3. Vaile, R. B., Jr., and Mills, L. D., LTJG, USN; "Evaluation of Earth Cover as Protection to Aboveground Structures"; Operation Teapot, WT–1128; Bureau of Yards and Docks, Washington, D. C.; Confidential Restricted Data.

4. Willoughby, A. B., Kaplan, K., and Condit, R. A.; "Effects of Topography on Shock Waves in Air"; Broadview Research and Development , WADC TR-56-289.

5. Sachs, D. C., Swift, L. M., and Sauer, F. M.; "Overpressure and Dynamic Pressure versus Time and Distance"; Operation Teapot, WT–1109; Stanford Research Institute, Menlo Park, California; Confidential Formerly Restricted Data.

6. Swift, L. M., Sachs, D. C., and Sauer, F. M.; "Air Blast Phenomena in the High Pressure Region"; ITR–1403; Stanford Research Institute, Menlo Park, California; Confidential Formerly Restricted Data.

7. Capabilities of Atomic Weapons, TM 23-200, July 1955; Department of the Army; Secret Restricted Data.

DISTRIBUTION

Military Distribution Category 5-22

ARMY ACTIVITIES

1 Asst. Dep. Chief of Staff for Military Operations, D/A, Washington 25, D.C. ATTN: Asst. Executive (R&SW)
2 Chief of Research and Development, D/A, Washington 25, D.C. ATTN: Atomic Division
3 Chief of Ordnance, D/A, Washington 25, D.C. ATTN: ORDTX-AR
4 Chief Signal Officer, D/A, P&O Division, Washington 25, D.C. ATTN: SIGRD-8
5 The Surgeon General, D/A, Washington 25, D.C. ATTN: Chief, R&D Division
6- 7 Chief Chemical Officer, D/A, Washington 25, D.C.
8 The Quartermaster General, D/A, Washington 25, D.C. ATTN: Research and Development
9- 12 Chief of Engineers, D/A, Washington 25, D.C. ATTN: ENGNB
13 Chief of Transportation, Military Planning and Intelligence Div., Washington 25, D.C.
14- 16 Commanding General, Headquarters, U. S. Continental Army Command, Ft. Monroe, Va.
17 President, Board #1, Headquarters, Continental Army Command, Ft. Sill, Okla.
18 President, Board #2, Headquarters, Continental Army Command, Ft. Knox, Ky.
19 President, Board #3, Headquarters, Continental Army Command, Ft. Benning, Ga.
20 President, Board #4, Headquarters, Continental Army Command, Ft. Bliss, Tex.
21 Commanding General, U.S. Army Caribbean, Ft. Amador, C.Z. ATTN: Cml. Off.
22- 23 Commanding General, U.S. Army Europe, APO 403, New York, N.Y. ATTN: OPOT Div., Combat Dev. Br.
24- 25 Commandant, Command and General Staff College, Ft. Leavenworth, Kan. ATTN: ALLL3(AS)
26 Commandant, The Artillery and Missile School, Ft. Sill, Okla.
27 Secretary, The U. S. Army Air Defense School, Ft. Bliss, Texas. ATTN: Maj. Gregg D. Breitegan, Dept. of Tactics and Combined Arms
28 Commanding General, Army Medical Service School, Brooke Army Medical Center, Ft. Sam Houston, Tex.
29 Director, Special Weapons Development Office, Headquarters, CONARC, Ft. Bliss, Tex. ATTN: Capt. T. E. Skinner
30 Commandant, Walter Reed Army Institute of Research, Walter Reed Army Medical Center, Washington 25, D. C.
31 Superintendent, U.S. Military Academy, West Point, N. Y. ATTN: Prof. of Ordnance
32 Commandant, Chemical Corps School, Chemical Corps Training Command, Ft. McClellan, Ala.
33 Commanding General, U. S. Army Chemical Corps, Research and Development Command, Washington, D. C.
34- 35 Commanding General, Aberdeen Proving Grounds, Md. ATTN: Director, Ballistics Research Laboratory
36 Commanding General, The Engineer Center, Ft. Belvoir, Va. ATTN: Asst. Commandant, Engineer School
37 Commanding Officer, Engineer Research and Development Laboratory, Ft. Belvoir, Va. ATTN: Chief, Technical Intelligence Branch
38 Commanding Officer, Picatinny Arsenal, Dover, N.J. ATTN: ORDBB-TK
39 Commanding Officer, Army Medical Research Laboratory, Ft. Knox, Ky.
40- 41 Commanding Officer, Chemical Corps Chemical and Radiological Laboratory, Army Chemical Center, Md. ATTN: Tech. Library
42 Commanding Officer, Transportation R&D Station, Ft. Eustis, Va.
43 Director, Technical Documents Center, Evans Signal Laboratory, Belmar, N.J.
44 Director, Waterways Experiment Station, PO Box 631, Vicksburg, Miss. ATTN: Library
45 Director, Armed Forces Institute of Pathology, Walter Reed Army Medical Center, 6825 16th Street, N.W., Washington 25, D.C.
46 Director, Operations Research Office, Johns Hopkins University, 7100 Connecticut Ave., Chevy Chase, Md. Washington 15, D.C.
47- 48 Commanding General, Quartermaster Research and Development, Command, Quartermaster Research and Development Center, Natick, Mass. ATTN: CBR Liaison Officer
49 Commanding Officer, Diamond Ordnance Fuze Laboratories, Washington 25, D. C.
50- 54 Technical Information Service Extension, Oak Ridge, Tenn.

NAVY ACTIVITIES

55- 56 Chief of Naval Operations, D/N, Washington 25, D. C. ATTN: OP-36
57 Chief of Naval Operations, D/N, Washington 25, D.C. ATTN: OP-03EG
58 Director of Naval Intelligence, D/N, Washington 25, D.C. ATTN: OP-922V
59 Chief, Bureau of Medicine and Surgery, D/N, Washington 25, D.C. ATTN: Special Weapons Defense Div.
60 Chief, Bureau of Ordnance, D/N, Washington 25, D.C.
61 Chief, Bureau of Ships, D/N, Washington 25, D.C. ATTN: Code 348
62 Chief, Bureau of Yards and Docks, D/N, Washington 25, D.C. ATTN: D-440
63 Chief, Bureau of Supplies and Accounts, D/N, Washington 25, D.C.
64- 65 Chief, Bureau of Aeronautics, D/N, Washington 25, D.C.
66 Chief of Naval Research, Department of the Navy Washington 25, D.C. ATTN: Code 811
67 Commander-in-Chief, U.S. Atlantic Fleet, U.S. Naval Base, Norfolk 11, Va.
68- 71 Commandant, U.S. Marine Corps, Washington 25, D.C. ATTN: Code A03H
72 President, U.S. Naval War College, Newport, R.I.
73 Superintendent, U.S. Naval Postgraduate School, Monterey, Calif.
74 Commanding Officer, U.S. Naval Schools Command, U.S. Naval Station, Treasure Island, San Francisco, Calif.
75 Commanding Officer, U.S. Fleet Training Center, Naval Base, Norfolk 11, Va. ATTN: Special Weapons School
76- 77 Commanding Officer, U.S. Fleet Training Center, Naval Station, San Diego 36, Calif. ATTN: (SPWP School)
78 Commanding Officer, Air Development Squadron 5, VX-5, U.S. Naval Air Station, Moffett Field, Calif.
79 Commanding Officer, U.S. Naval Damage Control Training Center, Naval Base, Philadelphia, Pa. ATTN: ABC Defense Course
80 Commander, U.S. Naval Ordnance Laboratory, Silver Spring 19, Md. ATTN: EE
81 Commander, U.S. Naval Ordnance Laboratory, Silver Spring 19, Md. ATTN: EH
82 Commander, U.S. Naval Ordnance Laboratory, Silver Spring 19, Md. ATTN: R
83 Commander, U.S. Naval Ordnance Test Station, Inyokern, China Lake, Calif.

84 Officer-in-Charge, U.S. Naval Civil Engineering Res. and Evaluation Lab., U.S. Naval Construction Battalion Center, Port Hueneme, Calif. ATTN: Code 753
85 Commanding Officer, U.S. Naval Medical Research Inst., National Naval Medical Center, Bethesda 14, Md.
86 Director, Naval Air Experimental Station, Air Material Center, U.S. Naval Base, Philadelphia, Penn.
87- 91 Chief, Bureau of Aeronautics, D/N, Washington 25, D.C. ATTN: AER-AD-41/20
92 Director, U.S. Naval Research Laboratory, Washington 25, D.C. ATTN: Mrs. Katherine H. Cass
93 Commanding Officer and Director, U.S. Navy Electronics Laboratory, San Diego 52, Calif.
94- 95 Commanding Officer, U.S. Naval Radiological Defense Laboratory, San Francisco, Calif. ATTN: Technical Information Division
96- 97 Commanding Officer and Director, David W. Taylor Model Basin, Washington 7, D.C. ATTN: Library
98 Commander, U.S. Naval Air Development Center, Johnsville, Pa.
99 Commander-in-Chief Pacific, Pearl Harbor, TH
100 Commander, Norfolk Naval Shipyard, Portsmouth 8, Va. ATTN: Code 270
101-106 Technical Information Service Extension, Oak Ridge, Tenn. (Surplus)

AIR FORCE ACTIVITIES

107 Asst. for Atomic Energy Headquarters, USAF, Washington 25, D.C. ATTN: DCS/O
108 Director of Operations, Headquarters, USAF, Washington 25, D.C. ATTN: Operations Analysis
109 Director of Plans, Headquarters, USAF, Washington 25, D.C. ATTN: War Plans Div.
110 Director of Research and Development, DCS/D, Headquarters, USAF, Washington 25, D.C. ATTN: Combat Components Div.
111-112 Director of Intelligence, Headquarters, USAF, Washington 25, D.C. ATTN: AFOIN-IB2
113 The Surgeon General, Headquarters, USAF, Washington 25, D.C. ATTN: Bio. Def. Br., Pre. Med. Div.
114 Asst. Chief of Staff, Intelligence, Headquarters, U.S. Air Forces-Europe, APO 633, New York, N.Y. ATTN: Directorate of Air Targets
115 Commander, 497th Reconnaissance Technical Squadron (Augmented), APO 633, New York, N.Y.
116 Commander, Far East Air Forces, APO 925, San Francisco, Calif. ATTN: Special Asst. for Damage Control
117 Commander-in-Chief, Strategic Air Command, Offutt Air Force Base, Omaha, Nebraska. ATTN: Special Weapons Branch, Inspector Div., Inspector General
118 Commander, Tactical Air Command, Langley AFB, Va. ATTN: Documents Security Branch
119 Commander, Air Defense Command, Ent AFB, Colo.
120-121 Research Directorate, Headquarters, Air Force Special Weapons Center, Kirtland Air Force Base, New Mexico, ATTN: Blast Effects Res.
122 Commander, Air Research and Development Command, PO Box 1395, Baltimore, Md. ATTN: RDDN
123 Commander, Air Proving Ground Command, Eglin AFB, Fla. ATTN: Adj./Tech. Report Branch
124-125 Director, Air University Library, Maxwell AFB, Ala.
126-133 Commander, Flying Training Air Force, Waco, Tex. ATTN: Director of Observer Training
134 Commander, Crew Training Air Force, Randolph Field, Tex. ATTN: 2GTS, DCS/O
135-136 Commandant, Air Force School of Aviation Medicine, Randolph AFB, Tex.
137-142 Commander, Wright Air Development Center, Wright-Patterson AFB, Dayton, O. ATTN: WCOSI
143-144 Commander, Air Force Cambridge Research Center, LG Hanscom Field, Bedford, Mass. ATTN: CRQST-2
145-147 Commander, Air Force Special Weapons Center, Kirtland AFB, N. Mex. ATTN: Library
148 Commander, Lowry AFB, Denver, Colo. ATTN: Department of Special Weapons Training
149 Commander, 1009th Special Weapons Squadron, Headquarters, USAF, Washington 25, D.C.
150-151 The RAND Corporation, 1700 Main Street, Santa Monica, Calif. ATTN: Nuclear Energy Division
152 Commander, Second Air Force, Barksdale AFB, Louisiana. ATTN: Operations Analysis Office
153 Commander, Eighth Air Force, Westover AFB, Mass. ATTN: Operations Analysis Office
154 Commander, Fifteenth Air Force, March AFB, Calif. ATTN: Operations Analysis Office
155 Commander, Western Development Div. (ARDC), PO Box 262, Inglewood, Calif. ATTN: WDSIT, Mr. R. G. Weitz
156-160 Technical Information Service Extension, Oak Ridge, Tenn. (Surplus)

OTHER DEPARTMENT OF DEFENSE ACTIVITIES

161 Asst. Secretary of Defense, Research and Engineering, D/D, Washington 25, D.C. ATTN: Tech. Library
162 U.S. Documents Officer, Office of the U.S. National Military Representative, SHAPE, APO 55, New York, N.Y.
163 Director, Weapons Systems Evaluation Group, OSD, Rm 2E1006, Pentagon, Washington 25, D.C.
164 Armed Services Explosives Safety Board, D/D, Building T-7, Gravelly Point, Washington 25, D.C.
165 Commandant, Armed Forces Staff College, Norfolk 11, Va. ATTN: Secretary
166 Commander, Field Command, Armed Forces Special Weapons Project, PO Box 5100, Albuquerque, N. Mex.
167 Commander, Field Command, Armed Forces Special Weapons Project, PO Box 5100, Albuquerque, N. Mex. ATTN: Technical Training Group
168-169 Commander, Field Command, Armed Forces Special Weapons Project, P.O. Box 5100, Albuquerque, N. Mex. ATTN: Deputy Chief of Staff, Weapons Effects Test
170-180 Chief, Armed Forces Special Weapons Project, Washington 25, D.C. ATTN: Documents Library Branch
181-185 Technical Information Service Extension, Oak Ridge, Tenn. (Surplus)

ATOMIC ENERGY COMMISSION ACTIVITIES

186-188 U.S. Atomic Energy Commission, Classified Technical Library, 1901 Constitution Ave., Washington 25, D.C. ATTN: Mrs. J. M. O'Leary (For DMA)
189-193 Los Alamos Scientific Laboratory, Report Library, PO Box 1663, Los Alamos, N. Mex. ATTN: Helen Redman
194-198 Sandia Corporation, Classified Document Division, Sandia Base, Albuquerque, N. Mex. ATTN: H. J. Smyth, Jr.
199-201 University of California Radiation Laboratory, PO Box 808, Livermore, Calif. ATTN: Clovis G. Craig
202 Weapon Data Section, Technical Information Service Extension, Oak Ridge, Tenn.
203-215 Technical Information Service Extension, Oak Ridge, Tenn. (Surplus)

UNCLASSIFIED